

# Chapter 5

## Properties and Testing of Printed Cement-Based Materials in Hardened State



**Jolien Van Der Putten, Venkatesh Naidu Nerella, Viktor Mechtcherine, Mélody D'Hondt, Mohammed Sonebi, Daniel Weger, Zhendi Wang, Constantino Menna, Nicolas Roussel, Dirk Lowke, Kim Van Tittelboom, and Geert De Schutter**

**Abstract** 3D printing is offering a totally new construction method, but an in-depth understanding of the consequences of the different production conditions compared to traditional formwork-based casting operations is required. Bulk material properties (intrinsic strength and durability) will follow the same fundamental material laws. However, in printed structures, the role of the interfaces will become increasingly important as they affect the mechanical performance, transport properties and durability behaviour. Additionally, the anisotropic nature of 3D printed structures

---

J. Van Der Putten (✉) · K. Van Tittelboom · G. De Schutter  
Department of Structural Engineering and Building Materials, Ghent University,  
Magnel-Vandepitte Laboratory, Technologiepark-Zwijnaarde 60, 9052 Ghent, Belgium  
e-mail: [Jolien.vanderputten@ugent.be](mailto:Jolien.vanderputten@ugent.be)

V. N. Nerella · V. Mechtcherine  
Technische Universität Dresden, Dresden, Germany

M. D'Hondt  
Centre Scientifique Et Technique du Bâtiment (CSTB), Division Structure, Maçonnerie et  
Partition, Champs-sur-Marne, France

M. Sonebi  
School of Natural and Built Environment, Queen's University Belfast, Belfast BT9, UK

D. Weger  
Ingenieurbüro Schiessl—Gehlen—Sodeikat GmbH, München, Germany

Z. Wang  
Institute of Concrete Science and Engineering, China Building Materials Academy, Beijing, China

C. Menna  
Università Degli Studi Di Napoli Federico II, Naples, Italy

N. Roussel  
Laboratoire NAVIER, Gustave Eiffel University, 5 Boulevard Descartes, 77420  
Champs-sur-Marne, France

D. Lowke  
Institute of Building Materials, Concrete Construction and Fire Safety, Technische Universität  
Braunschweig, Beethovenstr. 52, 38106 Braunschweig, Germany

implies that there are new opportunities to develop new methods of analysis. The aim of this chapter is to focus on the current practices for performance testing and to give an overview of the parameters which affect the hardened properties of a printed cementitious material.

**Keywords** Anisotropic behaviour · Mechanical properties · Durability · Microstructure

## 5.1 Introduction

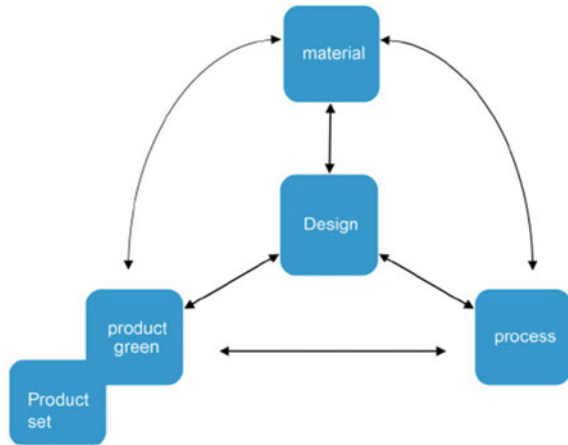
In recent years, 3D printing of concrete has become one of the emerging technologies that can minimize the supply chain in the construction (2017) process by automatically producing building components with complex geometries layer by layer, directly from a digital model without human intervention (Zareiyan and Khoshnevis 2017; Panda et al. 2018). Hence, to some extent, it could save material wastage, construction time and manpower on construction sites.

In general, 3D printing is already successfully applied in different sectors and with the use of different materials, for example, polymers. These materials are extruded in a liquid state and subsequently harden. The transfer to concrete, a material that undergoes a similar phase transition, seems obvious. However, in spite of a similar behaviour, there are some limitations and challenges concerning material properties and print processes that have to be faced in case of concrete printing (Wangler et al. 2016; Panda et al. 2017). Not only the complex characteristics of the material, such as shrinkage, creep, age-dependency, etc. will create many challenges and conflicting requirements, also the different production technique and the additional influence of print process and nozzle geometry will affect the mechanical performance of concrete compared with traditionally cast material.

Regardless of the application of this technique, there is always an interdependency between material, process and product (Fig. 5.1). This is even more pronounced in case of concrete, because of two reasons. First, the slow setting reaction in the printed concrete results in a strong interaction with the applied print parameters such as print speed and pump pressure. Secondly, concrete itself is not a single fixed material, but can have a wide range of compositions that may be more or less suitable in relation to the printing process and the required properties of the final product. Consequently, the print strategy cannot be chosen independently from the design, material or final product considerations (Bos et al. 2016).

In the following sections of this chapter, these specific challenges and pitfalls compared with the traditional way of casting concrete will be discussed.

**Fig. 5.1** Interdependency of design, material, process and product (Bos et al. 2016)



## 5.2 Additive Manufacturing: Challenges and Pitfalls

### 5.2.1 Anisotropy: Occurrence and Influencing Factors

In traditional casting, concrete is generally placed in one continuous pour in a form-work and subsequently vibrated afterwards to obtain a homogenous and isotropic structural element, having similar properties in different directions. However, in case of 3D printed concrete, the elements are build-up from different filaments and anisotropy will occur in the material due to the applied print process and as a consequence of interface properties between the different layers. However, there are currently no studies indicating that the anisotropy exists in the deposited bulk material, but the number of layers can be so dense that effectively anisotropic behaviour should be assumed, rather than that the reduced strength of the discrete layers should be considered.

The anisotropic behaviour of printed materials, fabricated with both extrusion-based techniques and binder jetting technologies, has already been investigated intensively (Panda et al. 2017; Nerella et al. 2019; Le et al. 2012a; Paul et al. 2018; Wolfs et al. 2019; Weger et al. 2016a). Focusing on the material properties in the hardened state, the directional dependency of the printed layers was taken into account by determining the mechanical properties in three different directions, as depicted in Fig. 5.2. First observations (Le et al. 2012a, b; Van et al. 2016; Feng et al. 2015) showed that in general, the material strengths are superior in horizontal direction (Orientation I, Fig. 5.2) and that the tensile strength in vertical direction (Orientation II, Fig. 5.2) is related to the bonding strength among the successive layers. Secondly, it was also noted that anisotropy primarily exists with regard to strength and that the interfaces become increasingly important as these interfaces govern the overall structural performance of the components, with the bulk material properties as the upper limit of the performance that could theoretically be achieved (Bos et al. 2016).

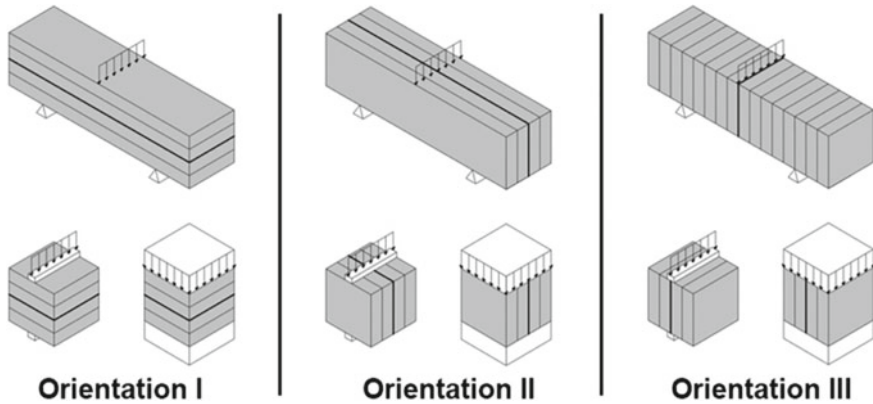


**Fig. 5.2** Directionally dependent mechanical testing respective to layer orientation of extrusion-printed concrete (Wolfs et al. 2019)

Another consequence of the anisotropic behaviour is the limited application of current structural design codes as these codes consider concrete as homogenous and do not take into account the effects of print process parameters. The classical concept of cube or cylinder testing as the basis for compliance testing will no longer hold, as moulded cube specimens cannot be obtained in the traditional way and would be not representative for 3D printed concrete. Durability indicator test methods (e.g. air permeability tests) will also need reassessments. Due to the porous interlayer zone, the air flow while performing an air permeability test will follow a preferential path, impairing the basic assumptions for the interpretation of the obtained pressure. Similar, in capillary suction tests, the results can be considerably affected by porous interlayer joints (Schröfl et al. 2019).

## 5.2.2 *Interlayer Time Interval*

As mentioned before, the interlayer is extremely important and the strength of this layer is expected to relate to a number of process parameters. A crucial print parameter is the interlayer time interval as it should be high enough to ensure enough strength during the print process. Moreover, a limitation of this delay time is required to ensure an adequate bonding between different layers. Several studies showed that an increased time interval results in a reduction of the interface strength and the compressive strength. Most investigations showed this strength reduction through simple macroscopically mechanical tests, but the findings are also supported by microscopical investigations by Van Der Putten et al. (2019) and Nerella et al. (2019), Venkatesh et al. (2017).

### 5.2.3 Print Process Parameters

Other influencing parameters related to the overall strength of the printed specimen have been investigated including printing path, print head speed and print nozzle height. Curing conditions also have a predominant influence on the anisotropy of the printed structure as discussed further in Sect. 5.2.6.2. Feng et al. (2015) investigated the mechanical properties of a layered structure, whereby a different print path was used in comparison to other investigations. In this research, every layer was a combination of different strips, printed next to each other as shown in Fig. 5.3. Preliminary results showed that the compressive strength is the highest in when testing Orientation I (Fig. 5.2). According to the printing process, the specimens can be seen as a lot of thin overlaying strips. The printing speed in this orientation is high, and the time of printing adjacent strips in Orientation II is much shorter than the time of printing adjacent layers in Orientation III.

The bond between two parts of the material appears to be higher when they are printed within a shorter time period, resulting in a higher strength inside a continuous strip than the one between strips, which is in turn higher than the strength between two layers. In these investigations, also the crack formation was observed during the compression tests. Feng et al. (2015) concluded that, when the specimens were loaded according to Orientation I, the cracks pass through inter-layer interfaces and strips. This observation is in contrast to specimens loaded in the second orientation, where the cracks pass through the inter-layer interfaces and inter-strip interfaces. Conducting the compression test according to Orientation III, the cracks pass through the inter-strip interfaces and inter-layer interfaces. As shown in Fig. 5.4, the crack surfaces have an angle of  $45^\circ$  (to the horizontal plane). The vertical path is slightly longer than the horizontal path, giving a higher strength in Orientation III because the inter-strip strength is higher than the inter-layer strength (Feng et al. 2015).

Feng et al. (2015) also investigated the influence on specimens fabricated on a structure where the different layers were printed in different strips (Fig. 5.3), and concluded that the deformation was not obvious until the maximum load was attained. Once this value was reached, the bottom of the specimen was cracked and this consequently led to a sharp drop in load. The observed failure modes could be

**Fig. 5.3** Structure of a 3D printed cubic specimen (Feng et al. 2015)

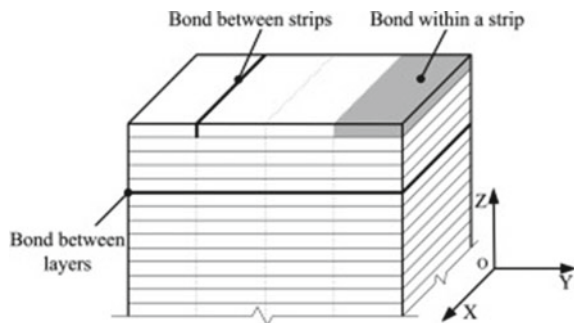
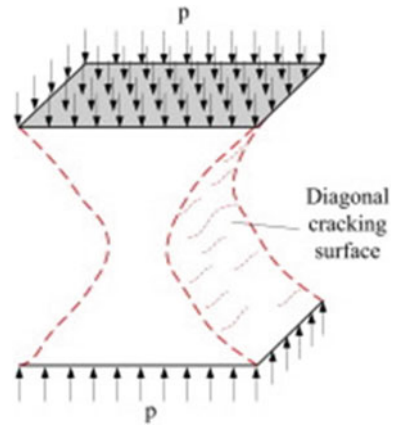


**Fig. 5.4** Failure mode of cubic specimens under compression (Feng et al. 2015)



divided into two main groups: First of all, when loading according to Orientation I, the cracks propagated suddenly through almost the whole section after cracking. However, in case of Orientation III, the crack developed slower compared with the ones in Orientation I, but the crack lengths were less than half of the cross-section depth correspondingly. Secondly, when loading occurs according to Orientation III, the position of the cracks was different and cracks appeared at the mid-section of the specimen. This in contrast with Orientation I, where the cracks deviated slightly from the middle to the part of the specimen printed late due to non-uniformity caused by the printing process.

The variation in results due to the influence of nozzle shape was observed by Bos et al. (2016) and Paul et al. (2018). Circular nozzles, as expected, create voids in the printed object and lower the strength. In the case of a rectangular or square nozzle, this problem may not be significant.

The differences in strength when applying a 3D printing technology can also be attributed to the direction-dependent compaction. Panda et al. (2017) and Sanjayan et al. (2018) postulated during their research that printed layers go through varying degrees of compression in various directions, resulting in corresponding compressive strength variation. On closer observations, two different types of compaction can be identified: (a) compaction in the extruder in the direction of the concrete extrusion and (b) compaction in deposited concrete by weight of the concrete layers deposited on top of it. These different compaction degrees result in different densities and consequently different mechanical properties.

The direction of deposition (i.e. vertically or horizontally), combined with nozzle-to-layer separation distance has a strong influence on the interlayer bond (Panda et al. 2018). While the horizontal deposition enables extrusion of layers with right-angled corners and smooth surfaces, as in the case of CONPrint3D (Mechtcherine et al. 2019), vertical deposition where new layers are “pressure-extruded” on to a substrate layer leads to better interlayer bonds and thus less anisotropy. It must be emphasized that the enhancement of bond most likely takes place only if the

concrete is extruded with flowrate higher than the required flowrate calculated as nozzle opening multiplied with nozzle-to-layer-height and print head velocity.

Lowke et al. (2015, 2018) showed that, by using binder activation methods, the application of the activator (water) influences the material properties. By spraying the water on the particle-bed surface (mixture of aggregates and binder, e.g. cement), the water will penetrate mainly driven by capillary forces. After spreading the next particle layer, the water also penetrates in the dry layer above. NMR measurements showed that there exists a water deviation between the layers, which leads to weak zones between the layers supposed due to a lower hydration. Experiments with a higher amount of water decreased this effect resulting in higher compressive and flexural strength of the material. Therefore, an application of the water with higher pressure or optimizing the packing density of the particle-bed to achieve an equal water distribution could lead to a better material performance.

### 5.2.4 Mix Composition

The anisotropy in printed structures is affected by the mix composition. More specifically, the water to cement ratio, binder volume, cement type (setting time), cementitious materials (silica fume, fly ash, etc.) particle size and shape, type of superplasticizer, viscosity modifying agent, etc. will affect the degree of anisotropy in case of printed specimens. One means by which the mix composition influences anisotropy is through rheological properties, which have a vital influence on the specimen geometry, deposition time interval and layer surface properties. Nerella et al. (2016) studied two different compositions, one with Portland cement as the sole binder, another with a binder consisting of Portland cement, fly ash and micro silica and the compressive strength was tested in different directions. They reported that the mixture containing high amounts of supplementary cementitious materials, showed superior performance in terms of both homogeneities of microstructure and low dependency of mechanical properties on the direction of loading when compared to mixture made with Portland cement as its sole binder. It is here noteworthy that the concrete composition determines its early age shrinkage. Early plastic and drying shrinkage values manifested as volumetric changes, especially in case of long time intervals, can lead to weak interface strengths and therefore to anisotropy in printed structures (Beushausen et al. 2007).

Another influencing component is the aggregate size and cement-to-aggregate ratio. The average compressive strength as a function of the before mentioned parameters are investigated by Zareiyan and Khoshnevis (2017) and are shown in Fig. 5.5. These results indicate that smaller sized aggregates, with consequently higher cement-to-aggregate ratio, yield to higher compressive strengths. The increase in compressive strength can be due to a decrease in aggregate volume relative to the total composite. The aggregate size also has an influence on the fracture surface. In general, failure under uniaxial compression occurs by debonding of the cementitious

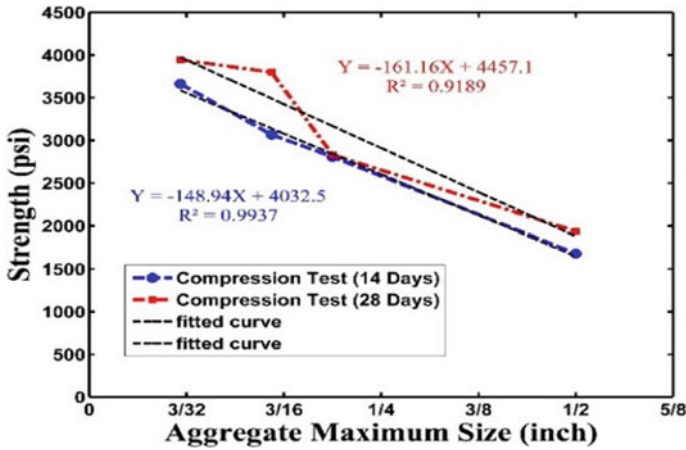


**Fig. 5.5** Compressive strength after 14 and 28 days for different maximum aggregate sizes (Zareiyan and Khoshnevis 2017)

mixture from aggregate particles. These micro-cracks form at the interface of aggregate. Therefore, cracks propagate around the aggregate rather than through it. This phenomenon is shown in Fig. 5.6. Composites containing large aggregates reveal a large number of cracks that propagates parallel to the loading axis. This is in contrast with smaller aggregates where gradual softening of the specimens resulted in the smoothest fracture surface and smaller (width, depth and length) cracks (Zareiyan and Khoshnevis 2017).

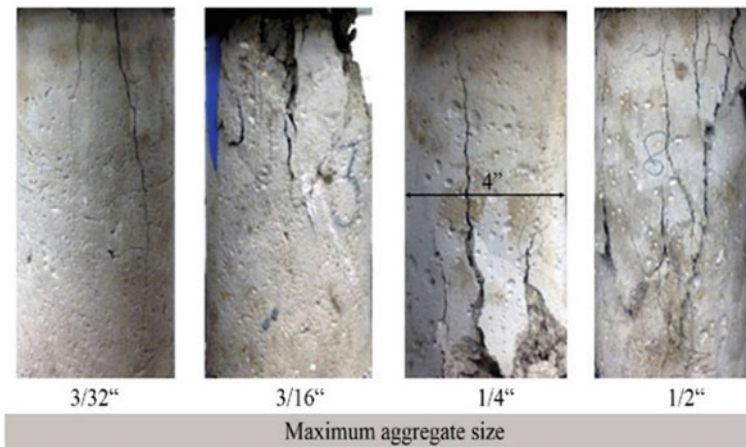


**Fig. 5.6** Surface fracture comparison of different maximum aggregate sizes (Zareiyan and Khoshnevis 2017)



Not only the compressive strength, also the flexural strength can be affected by the mix composition. In case of a high amount of supplementary cementitious materials, Nerella et al. (2019) reported a moderate strength reduction compared with a reference mixture with only Portland cement. These results stand for the most crucial test direction (Orientation III, Fig. 5.2), which means that the flexural strength values yield information on the tensile strength of the interlayer bond.

Weger et al. (2016a, b, 2018a, b) presented that, by using the particle-bed technology of the binder (cement paste) in combination with the flow resistance of the particle-bed (aggregate) determines the penetration behaviour of the binder. To provide sufficient strength and durability, the cement paste has to penetrate the particle layer completely, which needs at least a very low yield stress and viscosity. However, if the binder is too fluid with respect to the flow resistance of the particle-bed, the shape accuracy of the printed object will impair and the void content between the aggregates will increase again. Therefore, an optimum between the particle-bed flow resistance and the binder rheology has to be found (Weger et al. 2016a, b, 2018a, b; Lowke et al. 2018; Pierre et al. 2018).

### 5.2.5 Addition of Fibre

Reinforcement of the structure through fibre addition will try to tackle the inadequate tensile strength of the printed mortars. However, these fibres will affect the anisotropic behaviour of the material. Moreover, there are different fibre types with different properties and different behaviour available.

Rahul et al. (2019) investigated the mechanical behaviour of a 3D printed mortar including polypropylene (PP) fibres and compared the results with traditionally cast concrete. He observed that the bulk phase of the 3D printed mortar is denser than the corresponding mould cast specimen, due to the higher energy applied during the manufacturing process. The effect of his fibre addition on the anisotropic behaviour of the specimen was most pronounced in case of the bond shear strength, where in horizontal and vertical layers a strength reduction of about 24–25% and 22–30% was found compared with the traditionally cast specimen, respectively.

The compressive strength was not influenced by the fibre addition and similar results could be observed in all three testing directions. The results with respect to the flexural strength were inconsistent and highly dependent on the region where the samples were taken.

These results are inconsistent with the observations of Marchment et al. (2017), where the addition of PP fibres influenced the compressive strength positively when loading was applied perpendicular to the interface. He attributed this phenomenon to the preferential fibre alignment parallel to the direction of extrusion. The addition of fibres significantly enhanced the flexural performance of the printed samples. The use of fibre dosages equal to 0.75 and 1.00 vol% caused deflection-hardening behaviour of the 3D printed geopolymers as well as a higher fracture energy. However, an increase in fibre volume caused a minor reduction in interlayer bonding strength.

In the case of glass fibres, a slight reduction in compressive strength could be observed. This can be explained by the fact that glass fibres, located parallel to the loading direction, act like voids depending on the cement matrix ability to accommodate it in one of the three loading directions. Hambach and Volkmer (2017) on the other hand added three different types of fibres to his cementitious mixture: carbon, glass and basalt fibres. The diameter of the included fibres was equal to 7, 20 and 13  $\mu\text{m}$ , respectively. Two different print patterns, a parallel shaped and a crosshatch shaped pattern (Fig. 5.8), and two different test directions (Orientation I and III, Fig. 5.2) were employed in order to investigate the influence of different fibre types and changing fibre orientations along predetermined print paths. Preliminary results showed that, in case of a parallel print path, fibre type has no influence on the compressive strength when testing the specimens according to Orientation I. Testing the elements along Orientation II decreased the compressive strength from 80 to 30 MPa. In the case of a crosshatched shaped path, the same conclusions can be made (Hambach and Volkmer 2017) (Fig. 5.7).

Rubio et al. (2019) studied the effect of natural fibres (sisal) on the mechanical properties of a 3D printing mortar. They reported that triplicating the amount of sisal fibres did not affect the compressive strength and this conclusion could be drawn for both traditional cast cubes and layered specimens (Fig. 5.8). However, the

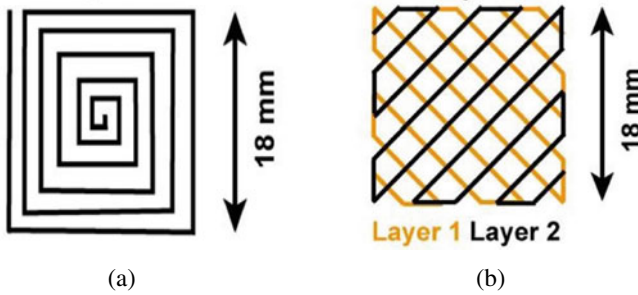
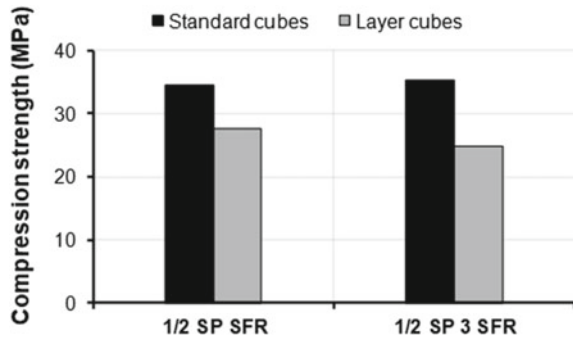


**Fig. 5.7** Top view of the printed paths for specimens used for uniaxial compressive strength: **a** parallel printing path and **b** crosshatch shaped path (Marchment et al. 2017)

**Fig. 5.8** Effect of adding different dosages of natural fibres (SFR) on the compressive strength at 7 days (Hambach and Volkmer 2017)



compressive strength of the layered cubes was approximately 25% lower compared to the standard cubes due to the inhomogeneity of the layered samples and the higher amount of entrapped air.

Based on the investigations of Hambach and Volkmer (2017), a decrease of approximately 25% in compressive strength is observed when comparing layered and standard cubes. This phenomenon can be explained by the heterogeneity of the layered cubes due to the lack of compaction and the higher amount of entrapped air.

## 5.2.6 Distinct Casting of Layers

### 5.2.6.1 Formation

As mentioned before, the interlayer time interval between two subsequent layers is a critical parameter and confronts the researchers with a paradox concerning the production rate of this particular process. On the one hand, the time gap between two deposited layers must be sufficiently long to provide adequate mechanical strength capable of sustaining the weight of the subsequently deposited layer. On the other hand, the time gap has to be short enough to ensure optimized bonding strength as well as building rate. Consequently, the optimum time gap should be the shortest that allows the stability of the layers during construction (Perrot et al. 2016).

Roussel and Cussigh (2008) reported a specific distinct-layer prevention methodology that may be relevant to the digital fabrication of concrete in fresh state: (1) the interface between two layers of fresh concrete must be rough; the roughness at the interface creates a (frictional) bond between two layers even if they do not mix and (2)  $A_{thix}$  of the first layer has to be low enough to allow the stresses generated at the interface between the two layers to re-initiate flow in the first layer. This research also showed that small amounts of accelerator can be used to achieve an increase in structuration which was mostly thixotropic (Roussel and Cussigh 2008; Di Carlo 2012).

High thixotropy may lead to an increase in the entrapment of air and the formation of lift lines in multilayer casting, which could reduce the bond strength. This reduced bond strength between two layers can create cold joints. These joints arise between successively cast layers of concrete that have limited intermixing. This can occur if a critical resting time is exceeded. The critical resting time depends on the density of the material, the gravitational force, the layer height, the structural build-up rate and the construction rate, as shown in Eq. (5.1) (Wangler et al. 2016; Roussel and Cussigh 2008).

$$t_c = \frac{\sqrt{\frac{(\rho gh)^2}{12} + \left(\frac{2\mu_p V}{h}\right)^2}}{A_{thix}} \quad (5.1)$$

With:

$t_c$	Critical value for the interlayer time interval	[s]
$\rho$	Density of the cementitious material	[kg/m <sup>3</sup> ]
$g$	Gravitational acceleration	[m/s <sup>2</sup> ]
$H$	Layer height	[m]
$\mu_p$	Plastic viscosity	[Pa.s]
$V$	Printing velocity	[m/s]
$A_{thix}$	Structuration rate	[Pa/s]

The properties of the interlayer in fresh state affect the mechanical behaviour of the element in the hardened state. To determine the interlayer bonding strength, test methods performed in the field of repair mortars serve as inspiration source. These different test methods are discussed more in-depth in section ‘Tensile strength’ but not all of them are applicable due to the different manufacturing process.

As the properties of the interlayer are extremely important, many researchers are investigating solutions to improve the interlayer quality and the solutions are mostly found in the field of repair mortars. However, as in the case of 3D printed mortars the bonding should be foreseen between two relatively fresh mortars, the behaviour is not completely the same and the number of influencing parameters will increase drastically.

Parameters that could have an influence on the interlayer bonding are:

- Surface preparation (and the possible use of bonding agents);
- Compressive strength of the weakest concrete layer;
- Moisture content of the substrate;
- Curing conditions;
- Additional voids;
- Stress state at the interface and the presence of cracking;
- Amount of steel reinforcement crossing the interface, among others.

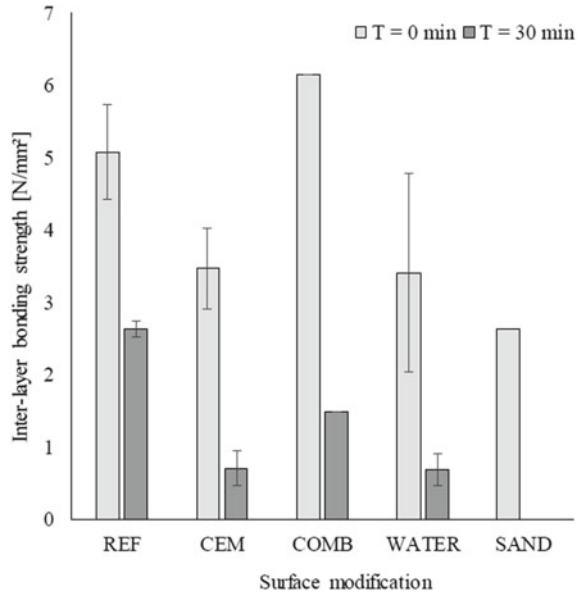
Considering the interface between two relatively fresh layers in 3D printing applications, the amount of influencing parameters will be extended when taking into account the print process itself. More specifically, the occurrence of chemical bonding as well as the effect of restrained shrinkage and a changing stiffness over time are phenomena that cannot be neglected. In the following sections, different surface preparation techniques are listed as a possible improvement of the interlayer quality.

### 5.2.6.2 Enhancement Methods

#### Surface Preparation

Previous research (Le et al. 2012a; Zareiyan and Khoshnevis 2017; Júlio et al. 2004; Santos et al. 2012) states that a higher surface roughness will lead to an increased

**Fig. 5.9** Interlayer bonding strength after different surface modification techniques (Van Der Putten et al. 2019)



bonding strength between the different concrete parts. However, as some researchers using nozzles equipped with trowels to flatten the substrate layer and to ensure a similar roughness over the entire length of the printed specimen, enhancement methods are required. A first possibility to increase the surface roughness is by adding sand particles in between two printed layers or by using nozzles with grooves. These techniques increase the surface roughness with 17 and 68%, respectively. Unfortunately, a similar trend could not be observed when comparing the interlayer bonding strength (Fig. 5.9) as only a nozzle with grooves (COMB, Fig. 5.9) improves the bonding when the time gap between the layers is equal to zero. The non-automated addition of sand particles deteriorates the bonding as it creates large cavities between the printed layers due to an inadequate attachment. The latter weakens the interface zone and results in a lower interlayer bonding strength. In the case of a 30 min time gap, complete de-bonding was observed.

Another enhancement method is performing topological interlocking, which is a design principle that holds the element together purely by geometrical constraints without using any binder or connector. Fabricating printed elements with interlocked parts will increase the bonding strength due to an increased contact surface between the layers until a certain depth of the particular interlock (Figs. 5.10 and 5.11).

The addition of fibres and the construction process (cast or extruded) can also influence the surface roughness of a printed element. Peled and Shah (2003) described the surface roughness of extruded composites with and without the addition of fly ash and after adding PVA fibres with different lengths. She detected that in case of extruded composites without fly ash and 2 mm fibres, a large number of long fibrils were lying on top of the fracture surface. These long fibrils will increase the roughness

**Fig. 5.10** Interlocking systems (Di Carlo 2012)

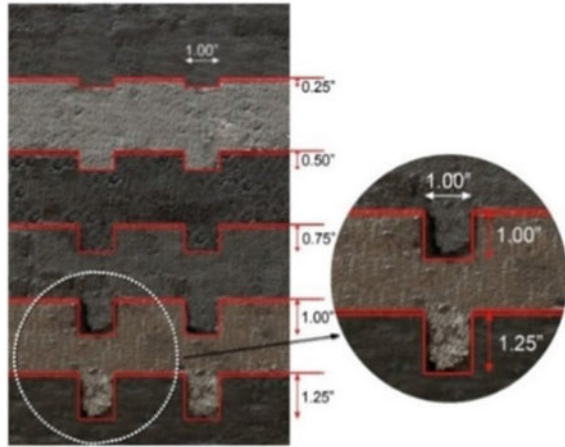
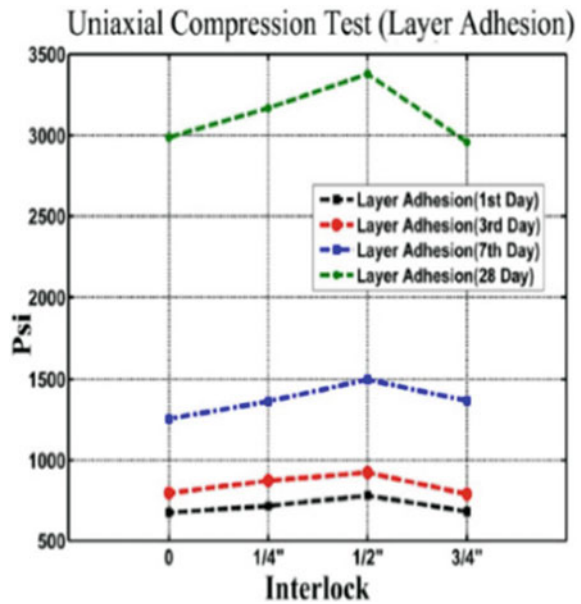


**Fig. 5.11** Bond interface of four types of interlock (Di Carlo 2012)



of the surface and indicate an aggressive pull-out process with high friction between the fibre and the cement matrix, suggesting a strong bond between the layers. In the extruded composite, also a layer of cementitious matrix is seen on the fibre surface, indicating that the de-bonding process is taken place not only at the fibre-matrix interface, but also in the matrix near the fibre.

## Moisture Content and Curing Conditions

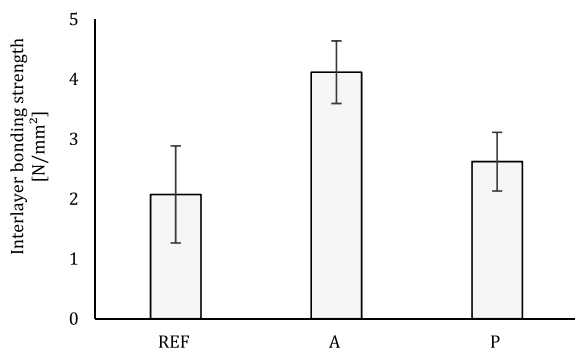
Moisture content of the substrate layer is a very specific issue and literature shows very contradictory results. In the first instance, Emmons and Emmons (1993) mentioned that an excessively dry substrate may absorb too much water from the overlay while excessive moisture in the substrate may clog the pores and prevent absorption of the overlay. Therefore, a saturated substrate with a dry surface will be considered as the best.

However, in case of printed elements, the moisture content of the substrate layer depends on the time gap between the printed layers and also in this case, the results are inconsistent. Sanjayan et al. (2018) observed that a layer interval of 20 min creates the lowest surface moisture content and consequently results in the lowest bonding between two subsequent layers compared to other time intervals (i.e. 10 and 30 min). On the other hand, Van Der Putten et al. (2019) reported a continuing decrease in moisture content for an increasing time gap and a similar trend could be observed for the interlayer bonding strength of the specimens. To overcome the problem of a drying interface, researchers moisturized the substrate layer just before printing the second layer after a predefined time gap. Unfortunately, the results were not as good as expected and the bonding between the layers could not be improved.

The addition of superabsorbent polymers (SAPs) is not only effective for a reduction in autogenous (Wyrzykowski et al. 2018) or plastic (Serpukhov and Mechtcherine 2015) shrinkage, it also has a positive effect on the interlayer bonding strength as reported by Van Der Putten et al. (2019). Due to the creation of a lower tensile stress and a prolonged moisture state of the interface, an increase in bonding strength could be observed for both smaller (SAP A) and bigger (SAP P) sized polymers (Fig. 5.12).

Curing conditions can also affect the bonding between the different layers. Storage of the specimens in laboratory environment will lead to a higher interlayer adhesion compared to specimens stored in outside conditions due to the changing relative humidity. Also curing immediately after the addition of the top layer and this for at least 3–7 days will improve the bonding strength (Santos and Eduardo Nuno Brito Santos 2011).

**Fig. 5.12** Interlayer bonding strength of a 3D printed cementitious material with two different sized SAPs (error bars represent the standard deviation) (Van Der Putten et al. 2019)



## Compressive Strength

Developing higher strength concrete is important because of its effect on bond strength. Beushausen and Alexander (2008) investigated the influence of the new concrete compressive strength on the shear bond between old and new concrete and they found a constant correlation between the two parameters. Neville (1995) also mentioned the increase in tensile strength was the result of an increase in compressive strength, but at a slower rate than shear. Thus, developing higher strength concrete resulted in better adhesion.

## Print Parameters

As mentioned in section ‘Cold joints’, the interval time between layer depositions has a great influence on the structural properties of the printed element. Poorly controlled time gaps result in cold joints at the interface and reduce the overall strength of the structure. To avoid a plane of discontinuity and eliminate long delays, the optimum time laps between the layers should be carefully determined. New layers must be added after the previous layer is sufficiently hardened and before it’s over cured. Therefore, the fabrication speed must be designed to allow layers to bond in a proper way.

In general, different researchers (Panda et al. 2018; Nerella et al. 2019; Le et al. 2012a; Van Der Putten et al. 2019; Tay et al. 2018) reported a decreasing adhesion between the layers with an increasing time gap. The same conclusions were made by Panda et al. (2018). Figure 5.13a shows the effect of an increasing time gap on the interlayer bonding strength of specimens made out of the same batch material. When the applied time gap exceeds the open time of the material, it becomes necessary to print elements with different batch material. The results are shown in Fig. 5.13b. In both cases, an increasing time gap will induce a lower strength.

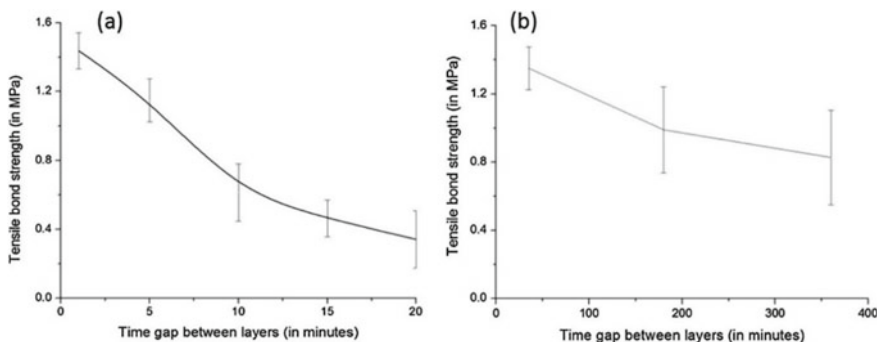


**Fig. 5.13** Effect of an increasing time gap on the interlayer bonding strength of specimens made out of **a** the same and **b** different batch of material (Panda et al. 2018)



Besides the time gap, also the mix composition and the number of layers will have an influence on the bonding strength. Zareiyan and Khoshnevis (2017) stated that mixtures with small aggregates lead to a higher split cylinder test (approximately 80%). The bonding of a four layer element compared with a monolithic part is in general 19% lower.

On the other hand, Sonebi et al. (2001) investigated the effect of the water-to-binder ratio in case of underwater concrete cast on old concrete used for underwater repair. Within this research, two types of binders were used. The first type was a combination of cement with silica fume (10%), while in the second type cement was combined with silica fume (6%) and fly ash (20%). Preliminary results showed that an increased water-to-binder ratio reduces the interlayer bonding and adhesion in slant shear strengths. More specifically, by increasing the water-to-binder ratio from 0.41 to 0.47, the adhesion values were reduced by approximately 40%. It was also reported that the combination of silica fume and fly ash exhibited the greatest adhesion in slant-shear in air and water compared to 100% cement mixture (Mohammed Sonebibond water-to-binder 2001).

### 5.2.6.3 Early Age Shrinkage

In general, shrinkage is one of the major issues for concrete elements as it will lead to unwanted deformations that affect the geometry, durability as well as the mechanical properties. Especially, when the deformations are restrained, shrinkage may lead to (tensile) stresses and cracking that degrade the quality of the printed specimen and increases the amount of preferential ingress paths for chemical substances. Shrinkage can be categorized according to two characteristics: time/duration and chemical and/or physical cause and different types of shrinkage can be distinguished. First of all, after placement and before final setting, a cementitious material subject to desiccation undergoes in fresh state volumetric deformations, referred to as plastic shrinkage. In this phase, the paste is still fresh and can be considered as solid particles suspended in cement–water. The printing environment (e.g. wind, high temperature, low humidity,...) might cause a rapid loss of water to the surroundings by evaporation. As 3D printed elements are manufactured without formwork, their surface area exposed to the environment is larger resulting in an acceleration of the plastic and drying shrinkage behaviour and an increased cracking risk (Fig. 5.14).

A possible solution to reduce plastic and/or drying shrinkage is curing. Both external and internal curing methods are adequate. Le et al. (2012a) showed the effect of the different external curing mechanisms on the early age drying shrinkage of printed specimens and compared them with shrinkage in sprayed concrete (Fig. 5.15).

It was shown that curing in water or damp hessian (burlap) can reduce shrinkage. When comparing the different curing methods, curing in water is the best technique to avoid shrinkage. These conclusions are not surprising, but it leaves the challenging question on how to practically cure 3D printed elements in an efficient and economical way. Manual curing was provided by constantly wetting the printed elements during the first day, which does not seem to be an optimal or efficient solution.



Fig. 5.14 Early age shrinkage cracking in 3D printed walls (Schröfl et al. 2019)

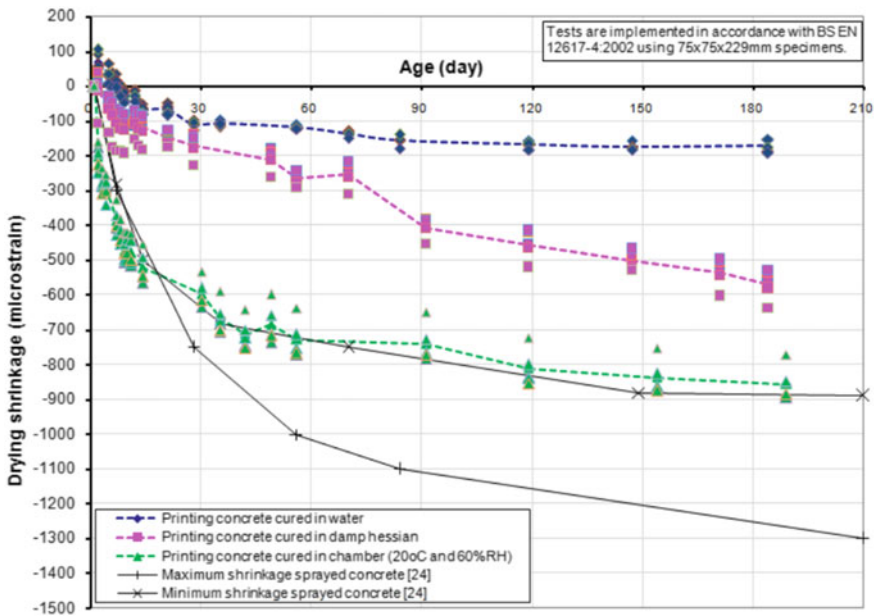


Fig. 5.15 Dry shrinkage in three curing conditions compared with sprayed concretes (Le et al. 2012a)

Internal curing can be obtained by including superabsorbent polymers (SAPs) in the mix design. Different researchers already demonstrated the positive effect of this addition on the shrinkage behaviour. First of all, Serpukov and Mechtcherine (2015) showed that the incorporation of superabsorbent polymers can mitigate plastic shrinkage cracking of both ordinary concrete and strain-hardening cement-based

composites (SHCC). These results were also confirmed during a RILEM inter-laboratory study (2019). Secondly, the addition of SAPs to reduce shrinkage is an ongoing research at Ghent University (Van Der Putten et al. 2019), where different types of polymers (i.e. different sizes but similar chemical composition) are mixed in a 3D printed mortar. After measuring both autogenous and unrestrained (free) shrinkage, preliminary results showed for both shrinkage types that smaller SAPs have the best prospective as they release the entrained water in a more gradual way. They also decrease the nanoporosity in the range of 100 to 500 nm, which is ascribed to a better hydration rate around the SAPs, closing up the smaller pores as well as to their autogenous shrinkage mitigation that reduces the amount of micro-cracking.

Another reason that induces a higher shrinkage risk is the mix composition of the printable mixture. In most 3D printable cementitious materials, the cement content is high to ensure rapid early age strength. This, combined with the lack of coarse aggregates, will induce a higher shrinkage risk. In order to obtain a more durable cementitious mixture, Zareiyan and Khoshnevis (2017) replaced ordinary Portland cement (OPC) partly by Calcium Sulphoaluminate Cement (CSA) and described this replacement as a possible solution to decrease shrinkage. Although CSA increases the concrete strength more rapidly than the concrete shrinkage stress, it also requires about 50% more water than OPC for hydration. As most of the water in the mixture is used for hydration, this replacement can negatively affect the autogenous shrinkage of the material. Further research on this is necessary.

Other researchers (Le et al. 2012a; Serpukhov and Mechtcherine 2015; Zingg et al. 2009; Mechtcherine et al. 2014) used fibres (steel fibres and polymeric microfibers respectively) to exploit their potential and their effect on shrinkage and deformation in plastic state. As their addition reduces the formation of fine cracks, they decrease plastic shrinkage cracking, resulting in a more durable material.

#### 5.2.6.4 Reinforcement

Printed cement-based materials are quasi-brittle like casted materials, but as they are often fine-grained they tend to be more brittle and their failure behaviour is mostly characterized by a low ratio of tensile to compressive strength and a low ultimate tensile strain compared to their fracture strain. Although this implies that fundamental structural behaviour of digitally fabricated reinforced elements will not differ from conventionally build reinforced elements, the fabrication of novel reinforced concrete structures using digital technologies necessarily requires the definition of suitable strategies for reinforcement implementation. The successful integration of existing reinforcement systems (steel rebar, rods, wires, fibres or filaments) will indeed allow for printed concrete structures to be designed using standard structural codes as the same type of reinforcement is used (material, reinforcement degree, position). However, as the integration of reinforcement has to be compatible with either the specific printing technique adopted for the structural element production as with the shape, more specific properties related to the print process (e.g. anisotropy, weak interfaces and reduced inter-layer bonding) also have to be considered (Asprone et al.

**Table 5.1** Grouping of possible approaches to address reinforcement integration in DFC (Asprone et al. 2018)

<u>By structural principle</u>	
Ductile printing material <i>e.g. fibre reinforced materials</i>	Rebar reinforcement is not required and fibres are able to provide the tensile strength and the ductility that are required by the application
DFC composite: <i>e.g. passive reinforcement</i>	Rebar reinforcement is needed and it can also be installed with automated/robotized processes
Compression load structures <i>e.g. due to shape or pre-stress</i>	Additional tensile reinforcement is not required
Hybrid solutions <i>e.g. combining any of the previous cases</i>	
<u>By stage of the manufacturing process</u>	
Before manufacturing	Reinforcement is arranged and placed in the final configuration before concrete deposition through a digital fabrication method
During manufacturing	Reinforcement is added during concrete manufacturing or belongs to the material itself (e.g. fibres)
After manufacturing	Reinforcement is installed once the concrete element has been manufactured through a digital fabrication method

2018). The different ways of implementation can be classified by structural principle or by place in the manufacturing process, as listed in Table 5.1 (Asprone et al. 2018).

The most basic approach is to use the printed concrete not as the primary structural material, but rather as a formwork into which conventional steel reinforcement bars are positioned and which is subsequently filled with cast concrete. An alternative construction way is to place the reinforcement first and subsequently deposit the concrete around it. This approach is applied in the Smart Dynamic Casting (SDC) (Lloret et al. 2017) project, in which a dynamic formwork slip-forms the geometry around a pre-placed reinforcement mesh. An updated version of this technique is the application of Mesh Moulding (MM), a digital fabrication technique in which the reinforcement and formwork are unified in a robotically controlled system (Hack et al. 2017; Hack and Lauer 2014). With this technique, conventional deformed bars in grid form (40 × 40 mm) with diameters equal to 4.5 or 6 mm are used and the concrete is continuously cast in the core of the structure, reducing the potential layering issues.

Other developments aim to create reinforcement methods that are integrated during the printing process and the most advanced technique is currently under development at the TU/e, where a reinforcement cable is directly entrained during printing. This wired reinforcement type is not only strong and ductile, but also very flexible to produce concrete elements with complex geometries. Several experiments have already been conducted, using three different galvanized cables with ultimate tensile loads and diameters ranging from 420 to 1925 N and 0.63 to 1.20 mm respectively, having a significant ductility. However, due to the layered print process, cable slippage was a dominant failure mechanism when higher strength cables were applied.

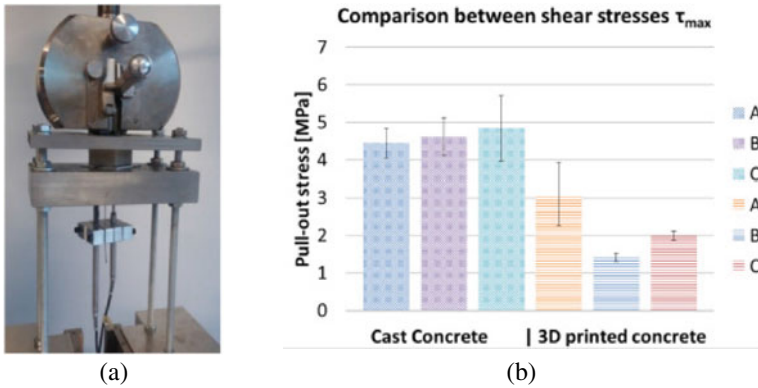


**Fig. 5.16** Pull-out test on concrete with embedded reinforcement cable: **a** experimental set-up with printed specimen, **b** comparison of average bond strengths in cast and printed concrete for 3 different cables (Bos et al. 2017)

This could be attributed to the poorer concrete compaction around the cables and the induction of peak stresses at the loaded side of the cables, inducing gradual debonding before the cable strength was fully reached. As can be seen in Fig. 5.16, the shear stress of printed specimens, based on pull-out tests, is only one third of the shear stress measured in case of cast concrete and is also lower than the calculated values.

The differences between the calculated values, based on model codes, and the experimental results can be attributed to the design model and the fact that these basic models are primarily based on the concrete quality, with some additional parameters accounting for various conditions. For instance, Eurocode2 (EC2) defines the design bond strength based on Eq. (5.2):

$$f_{bd} = 2,25 \cdot \eta_1 \cdot \eta_2 \cdot f_{ctd} \tag{5.2}$$

where  $\eta_1$  depends on the embedment quality,  $\eta_2$  on the reinforcement diameter, while  $f_{ctd}$  is the design tensile strength of the concrete. However, as listed below, the conditions for reinforced printed concrete are rather different for normal cast concrete and different parameters related to the printing process are not taken into account.

- The strength class and maximum grain size of printed mortars is significantly lower than the ones applied in case of ordinary structural concrete buildings;
- The stress–strain behaviour of the cables differs from the normal reinforcement steel bars, indicating a higher linear elastic strength limit and a lower stiffness;
- A smooth cable surface and lower dilatancy resistance, which influences the proportion between adhesive and dilatancy resistance;
- In normal calculation models, concrete is considered as homogeneous while printed mortars behave in an anisotropic way. The print process will also induce

a higher amount of voids and air bubbles, resulting in a poorer bonding strength and adhesion between both components;

- The required limitations (e.g. minimal diameter and minimal embedment length) can often not be achieved due to the geometrical limitations of the printed element.

In spite of the many advantages of this technique, the main drawback remains the orientation of the reinforcement that is necessarily in the direction of the printed filament. A possible way to cope with the geometrical freedom is the combination of printed concrete and steel by using gas-metal arc welding (Mechtcherine et al. 2018). Although this technique shows high potential, preliminary results showed that the printed steel bars exhibit a yield stress and tensile strength of approximately 20% less, but they also received a higher strain capacity compared with conventional reinforcement bars. The bonding between the printed steel bars and the concrete was comparable with the bonding performance of conventional steel bars. Microstructural investigations of the fracture surfaces showed less ductile regions in case of printed elements, probably caused by the rapid cooling of the melted metal during the welding process (Mechtcherine et al. 2018).

A third possibility to introduce passive reinforcement is to integrate it with the concrete after the fabrication process. The external reinforcement makes it possible to incorporate a higher amount of steel reinforcement. The preliminary outcomes of the experimental activities carried out so far have demonstrated that the initial flexural stiffness of the printed RC beam is comparable with an equivalent RC beam, whereas the overall nonlinear flexural behaviour is influenced by local failure mechanism, i.e. shear damage at the interfaces and steel–concrete anchoring failure. For a limited number of structural applications there are other possibilities to overcome the necessity of tensile capacity and ductility by designing structures loaded in compression only or by the application of a certain pre-stress. The latter has a broader application range due to its capacity to counteract tensile stresses. However, the application of a certain pre-stress limits the form of freedom and introduces an additional step in the manufacturing process.

Another possibility is mixing a certain amount of short fibres into the cementitious material before deposition. This is well known as a straight forward and efficient way to considerably enhance the mechanical performance of concrete. Researchers investigated different types of fibres (e.g. carbon fibres, glass fibres, basalt fibres) with different lengths and volume%. In fresh state, a strong alignment of these fibres in the direction of the flow due to extrusion process could be observed. In the hardened state, a higher flexural strength and tensile strength could be obtained (Le et al. 2012a; Nematollahi et al. 2018; Christ et al. 2015).

Nematollahi et al. (2018) investigated the effect of polypropylene (PP) fibres (0.25 and 1.00 vol%) on the properties of a 3D printed fibre reinforced geopolymer mortar. Fibre addition influenced the compressive strengths positively only when loading was applied perpendicular to the interface. This phenomenon can be traced back to the preferential fibre alignment parallel to the direction of extrusion. The addition of fibres significantly enhanced the flexural performance of the printed samples. The use of fibre dosages equal to 0.75 and 1.00 vol% caused deflection-hardening behaviour

of the 3D printed geopolymers and higher fracture energy. However, an increase in fibre volume caused a minor reduction in interlayer bonding strength.

With respect to the structural performances, the use of strain-hardening cement-based composites (SHCC) is particularly promising (Curosu et al. 2017). Under uniaxial tensile loading, SHCC exhibit quasi-ductile behaviour with a strain capacity up to several percent, resulting from the formation of multiple fine cracks prior to reaching the tensile strength of the composite. Ogura et al. (2018) developed and characterized a series of printable SHCC containing 1.00% to 1.50 vol% of high-density polyethylene (HDPE) microfibers. The specimens extracted from the printed walls exhibited multiple fine cracks and pronounced strain-hardening characteristics under uniaxial tensile loading, even for fibre volume fractions as low as 1.00 vol%. In fact, the strain-hardening characteristics of the printed elements were superior to those of mould-cast SHCC specimens (Fig. 5.17). However, the mechanical performance of printed SHCC in the direction perpendicular to layer-to-layer interfaces is expected to be much less convincing. The anisotropic behaviour and possible mitigating measures should be investigated in detail both for SHCC and other FRC in the context of digital concrete (Fig. 5.18).

A new technique, developed at China Building Materials Academy and the university of Catalonia, uses staplers as reinforcement. As the printer head includes both a printing nozzle and a stapler, the reinforcement and printing process occurs simultaneously and in a periodical manner. The stapler pushes a wire profile into the printed clay for a half a layer deep and these staples profiles form an over mesh structure (Wang et al. 2018). The big advantage of this technique is that the staples profiles form an overall mesh structure that fuses the printed layers together and compliments the overall structural soundness of the print. Integration of this process in large scale 3D concrete printing industry could push the geometrical limits of what could be realized (i.e. increased printing height and inclination maximum, better support for openings,..) as different geometries of staplers can be used (kumarji and Geneidy 2019).

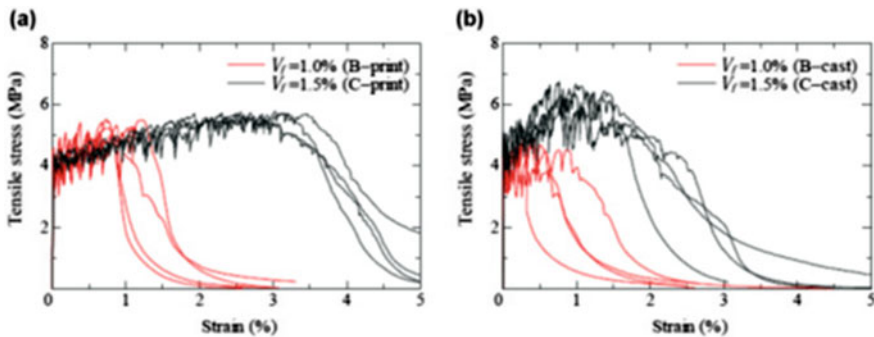


**Fig. 5.17** Stress–strain curves obtained from uniaxial tension tests on **a** printed specimens and **b** mould-cast specimens (Ogura et al. 2018)

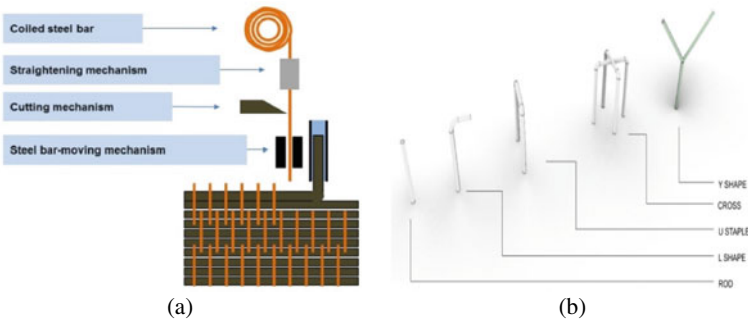


**Fig. 5.18** Simultaneous reinforcement of concrete while 3D printing: **a** Schematic diagram of reinforcement (Wang et al. 2018), **b** Different sized stapler geometries (Kumarji and Geneidy 2019)

### 5.3 Sampling and Quality Control

To measure the mechanical properties and to control the quality of printed elements, different specimens were saw cut from an original printed element and mostly compared with traditionally cast concrete elements, as shown in Fig. 5.19. In Le et al. (2012a), cubes, cylinders and prisms with different dimensions were taken from a 3D printed structure and tested in three loading directions (parallel to the side surface, parallel to the printing surface and parallel to the cut surface) to investigate the anisotropic behaviour (Bos et al. 2016).

Depending on the type of printing processes, voids of various magnitudes can form between the filaments, affecting the hardened properties and decreasing the overall structural stability. The shape of the filament has a significant influence on the voids at the layer-interfaces, with circular filaments leading to intrinsic voids

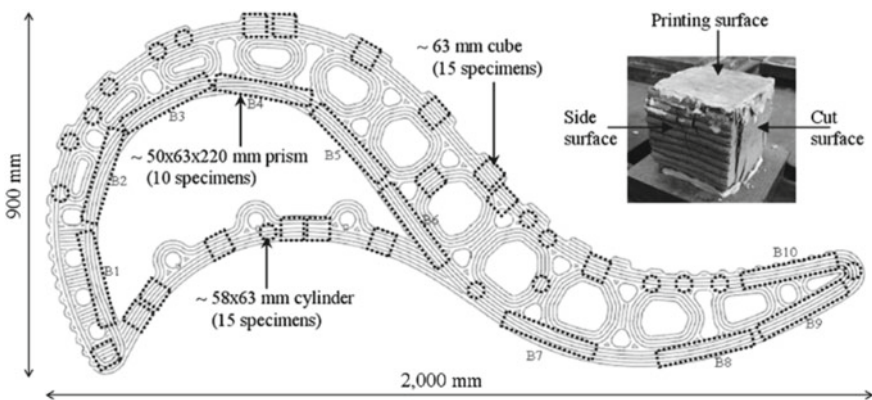


**Fig. 5.19** Diagram showing positions of extracted printed specimens (Le et al. 2012a)



between the layers (Fig. 5.20). Voids can also form due to feeding irregularities, deposition inaccuracies (e.g. nozzle oscillations) and inadequate rheology. Therefore, void measurements based on image analysis can be used to control the quality of the extracted concrete and to classify them in different categories as shown in Fig. 5.20. In mould-cast concrete, the amount of voids ranging from 0.2–4.0 mm size was 3.8%. In poorly printed concrete, the amount of voids was higher (4.8%) and in case of well printed specimens, only 1% voids were measured (Fig. 5.21).

Weger et al. (2018a, b) showed that the density (or porosity) of objects manufactured with the particle-bed based 3D printing method selective paste intrusion (SPI) depends on the penetration behaviour of the cement paste into the particle-bed. That penetration behaviour is affected by the mutual interaction of the rheological and thus the flow properties of the binder (cement paste) and the flow resistance of the particle-bed (aggregates). As the binder penetrates the layers of the aggregate sufficiently, the density of the material achieves values between  $2200 \text{ kg/m}^3$  and  $2400 \text{ kg/m}^3$ , comparable to normal mould-cast concrete specimen. However, as the binder shows insufficient penetration, the density decreases (porosity increases) which results in decreased strength and durability performance. Furthermore, Weger et al. (2018a, b) showed that the density of the specimens is a proper value to control the production quality (penetration ratio) of SPI objects, see Fig. 5.20.

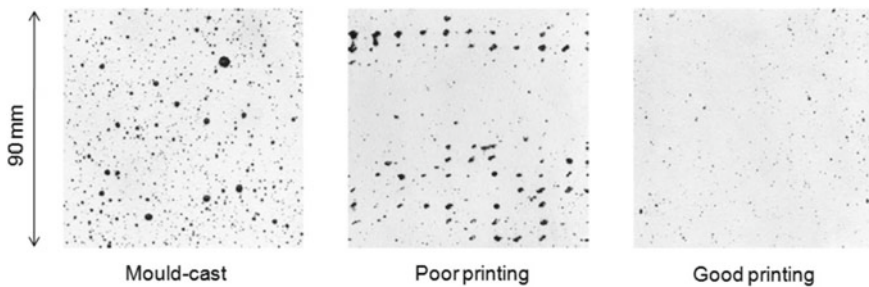


**Fig. 5.20** Quality control based on voids measurements (Le et al. 2012a)

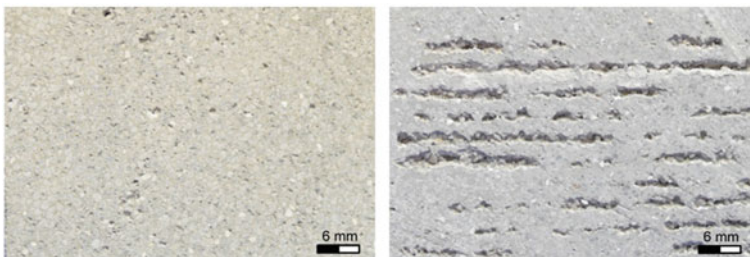


**Fig. 5.21** The particle-bed based 3D printing method selective paste intrusion. Cut through a cross section, left: with sufficient penetration of the layers of the particle-bed by the cement paste, right: with a non-sufficient penetration resulting in a decreased density and increased porosity (Weger et al. 2016a, b, 2018b)

**Table 5.2** Dimensions and binder type of the samples used for mechanical testing of 3D printed structures (Le et al. 2012a; Wolfs et al. 2019; Van Der Putten 2019; Rahul et al. 2019)

Filament [mm]	Compression (Cube size) [mm]	Tensile bond [mm]	Beam (Flexural) [mm]	Beam (Shrinkage) [mm]	Bindertype
Ø 9	100	Ø 58	100 × 100x400	75 × 75x229	CEM I, FA, SF
Ø 25	50		40 × 40x160		GP
20 × 20 30 × 15		~ 30 x ~ 90			FA/GP
			6 × 12x60		OPC, SF
			300 × 50x80		
			25 × 25x120		OPC

## 5.4 Mechanical Performance of 3D Printed Specimens

### 5.4.1 Measurements

Printed materials can be as good and as strong as cast material and it is possible to achieve materials with a higher density than cast equivalents, however the reproduction of ‘as good as cast’ properties on a commercial manufacturing scale has yet to be demonstrated. Creating solid objects from a conglomeration of extruded filaments predisposes printed objects to anisotropy, which influences end use performance.

Table 5.2 provides details of the papers that have investigated hardened properties as they are affected by filament bonding. Samples tended to be saw cut, or cored from printed materials.

There is no consistent format for describing the printing process parameters such as nozzle size, layer height, filament dimensions, print speed, component size from which the layers are taken or layer cycle times but all of them will have an influence on the mechanical properties and require to be taken into account when measuring and analysing the mechanical properties. The discrepancy in reporting process parameters and the variability in test geometry reported in Table 5.2, demonstrate the need for standardized testing methods as they exist in case of normal cast concrete. In the sections below, an overview of the test methods used for characterization of the mechanical performance of printed material can be found.

### 5.4.2 Compressive Strength

Most research groups (Panda et al. 2017; Le et al. 2012a; Paul et al. 2018; Le et al. 2012b; Van Zijl et al. 2016; Feng et al. 2015; Shakor et al. 2017) determine the compressive strength of printable concretes by means of a uniaxial compression test

on cubic or cylindrical specimens, similar to traditionally cast concrete. To examine the effect of the layered structure and the anisotropic behaviour, different testing directions are taken into account as mentioned in Section ‘Anisotropy’.

Many researchers reported anisotropy in compressive strengths (Panda et al. 2017; Nerella et al. 2019; Marchment et al. 2017). In addition to the mixture composition, compressive strength of printed elements depends on deposition time interval, process parameters and testing setup. Panda et al. (2019) and Sanjayan et al. (Wyrzykowski et al. 2018) explained the anisotropic behaviour of printed elements under compression loading using a hypothesis based on direction-dependent compaction. Nerella et al. tested printed specimens under compression in three loading cases (Fig. 5.22). A consistent conclusion based on these measurements could not be drawn, but the highest compressive strength was obtained in direction Par2 (Fig. 5.22, Orientation III Fig. 5.2). Although the differences in measured strengths were not very pronounced, they could be explained based on two phenomena:

- Differential water evaporation;
- Different failure criteria;

In addition to the uniaxial compression tests, Nerella et al. (2019), Venkatesh et al. (2017) hypothesized that the extent of the (weak) interface area lying outside the tri-axial compressive core and the size of individual defects (weak) interfaces lying in the crossing of shear planes are factors decisive for the observed load level at failure. In the specimens they investigated, the weak interface area outside the tri-axial compressive zone is the largest in case of a perpendicular loading (Orientation I, Fig. 5.2), which may explain why the strength values measured in these directions are the lowest. Another cause for the anisotropic behaviour of printed elements under compression loading is the varying degrees of compression that printed layers

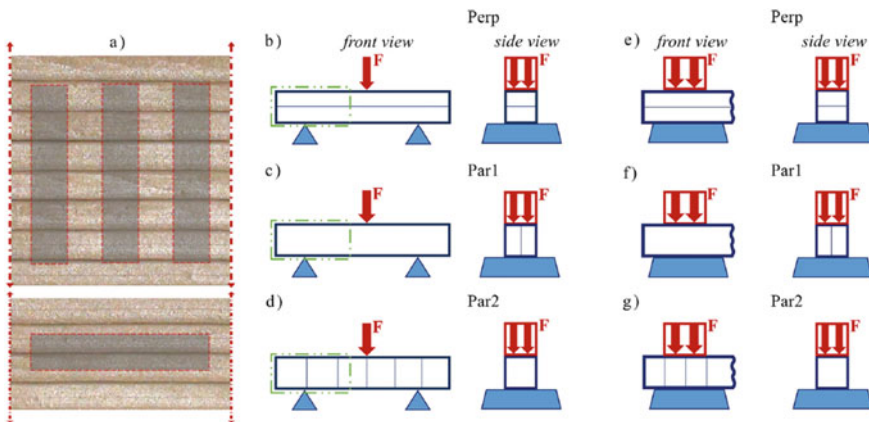


**Fig. 5.22** Representation of specimen extraction from a printed concrete wall as reported by Nerella et al. (2019)

go through in various directions, resulting in corresponding compressive strength variation (Sanjayan et al. 2018).

### 5.4.3 Flexural Strength

Another parameter in defining the mechanical behaviour of a specimen is measuring the flexural strength. Most researchers (Panda et al. 2017; Le et al. 2012a; Paul et al. 2018; Van Zijl et al. 2016; Feng et al. 2015) determine this parameter by means of a 3-point bending test on prismatic specimens, again very similar to traditionally cast concrete. To examine the effect of the layered structure and the anisotropic behaviour, different testing directions are taken into account (Fig. 5.2).

Rahul et al. (2019) proved the dependency of the flexural strength on the region subjected to the maximum bending moment in the three-point bending test. When tested along Orientation I, the maximum bending moment and corresponding maximum flexural stress occurs at the interface and showed values that were 32% lower. However, in case of parallel testing (Orientation II/III), a flexural strength increase of 20% could be observed as the maximum flexural stress.

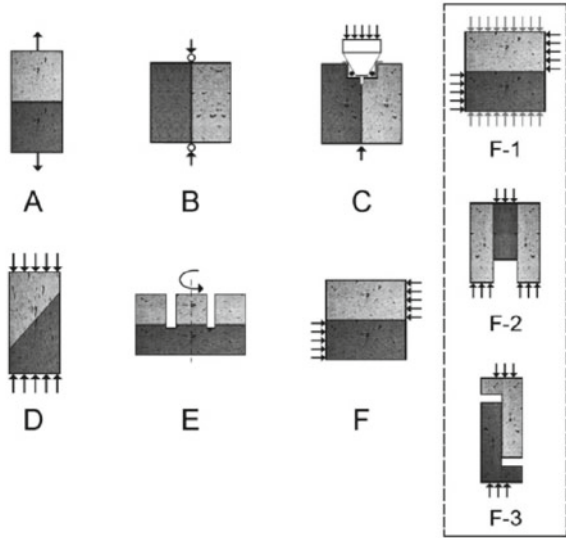
Lowke et al. (2015) showed flexural strength up to 5.3 MPa (Orientation I, Fig. 5.2) using the particle-bed based 3D printing method selective binder (cement) activation. The achieved flexural strength values were strongly connected to the water distribution between the layers.

### 5.4.4 Tensile Strength (Inter-Layer Bonding Strength)

To produce homogeneous structures and to ensure the structural stability, bonding between the different layers is considered as one of the key parameters. In case of a weak interface, cold joints can appear which can induce mechanical strength loss of more than 40% and a local increase of the porosity (Roussel and Cussigh 2008).

To understand bond mechanisms, it is essential to measure bond strength at the interface between new and old layers. A lot of test methods are developed for measuring the bond strength of old and new concrete. These test results vary substantially based on loading rate, specimen size, experimental set-up, etc. The existing methods can be divided into several categories. The first category measures the bond under tensile stress. The most common test set-up in this category is the pull-off test (ASTM D7234-05, Fig. 5.23A). This test evaluates the bond strength in tension of the interface and is highly dependent on the eccentricity of the applied load. Consequently, the results of this test method can be very scattered. When the tensile strength is lower than the bonding strength, the specimen will break at the layers and quantifying interlayer adhesion is not possible. Another test method in this category is the splitting test (ASTM C496, Fig. 5.23B). This test has a higher efficiency compared with the pull-off test because only a very small part of the bonded plate is

**Fig. 5.23** Interface bond strength test methods (Di Carlo 2017)



subjected to the maximum stress. An extension of the latter is the wedge splitting test (Fig. 5.23C). In this case, the interface strength is measured by fracture mechanics parameters (tensile interface strength and fracture energy).

The second category measures the bond under shear stress and is called direct shear methods. An example of this is the direct shear test (Fig. 5.23F). The bond surface is subjected to shear stress and small bending stress. The smaller stress concentration leads to a smaller scatter in test results. The third category is the one that combines shear and compression. An example of this one is the slant shear test according to ASTM C882/C882M (Fig. 5.23D). This test set-up uses a square prism or a cylindrical sample made of two identical halves bonded at 30° or 45° and tested under axial compression. During loading, the interface surface is under compression.

The choice of a proper bond strength test method is crucial, and different test methods cause distinct interface stress conditions in specimens. Consequently, the test results will differ when comparing different test methods. Literature shows that the measured bond strength decreases with the test method in the following order: slant shear, direct shear, splitting and pull-off (Aysha et al. 2014). The appropriate test for a particular case is the one for which the nature of loading is the most similar to that of stress conditions of the actual structure.

In case of 3D printing of concrete, the interlayer adhesion between the layers can be measured by applying pull-off tests (Zareiyan and Khoshnevis 2017; Panda et al. 2018; Le et al. 2012a; Zareiyan and Khoshnevis 2017) equipped with cubic or cylindrical specimens, saw cut or drilled from an original printed element. During these measurements, researchers reported the importance of failure in the interlayer and a very specific specimen preparation is required. First of all, high deviations on specimen dimensions should be avoided as they result in a high scatter due to the rather small specimen size. The alignment of the specimens in the test equipment is

also an important factor in order to avoid bending moments and measure only the bonding between the layers.

An updated version of the pull-off tests is developed and reported by Rahul et al. (2019) as depicted in Fig. 5.24. The interface of the specimen is placed horizontally in the grooves of upper and lower jaws of fixture. The jaws were then pulled apart at a constant displacement rate (i.e. 0.1 mm/min). The failure is divided by the cross-sectional area of the cylinder to obtain the bond shear strength. To induce only tensile stresses at the bonding area, Liu et al. (2019) developed a new method called cross-bonding (Fig. 5.25). This method enables the evaluation of both tensile strength and interfacial shear strength. In addition with this method, a decreasing trend in interlayer bonding strength could be observed in case of an increased interlayer time interval.

When comparing different test methods for measuring the bond strength, two distinctive failure modes (in cast specimens) can be observed: adhesive and cohesive failure. Adhesive failure or interface de-bonding occurs at the interface whenever the bond strength is reached. Due to mechanical interlocking, small particles were observed at the interface of these failed specimens. On the other side, cohesive failure occurs in the bulk by concrete crushing. Figure 5.26 gives an example of

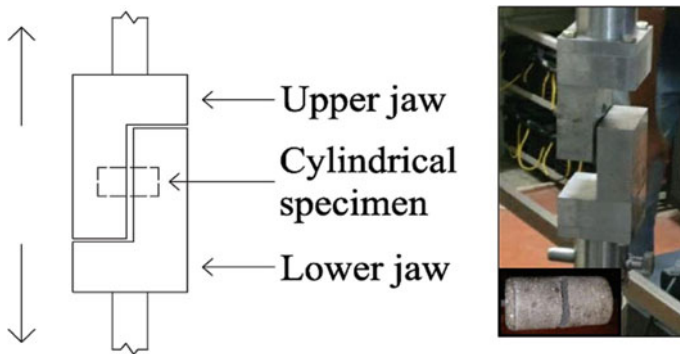


Fig. 5.24 Fixture for bond shear test (Rahul et al. 2019)

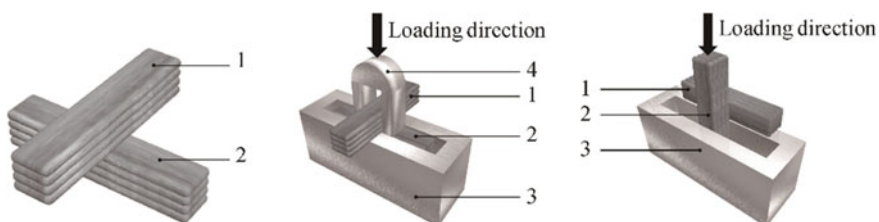
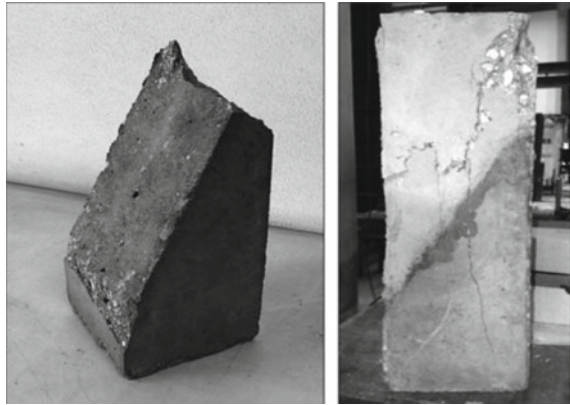


Fig. 5.25 Cross-bonding method (1. Upper printed block, 2. Bottom printed block, 3. Bed frame, 4. U-type loading head) (Liu et al. 2019)

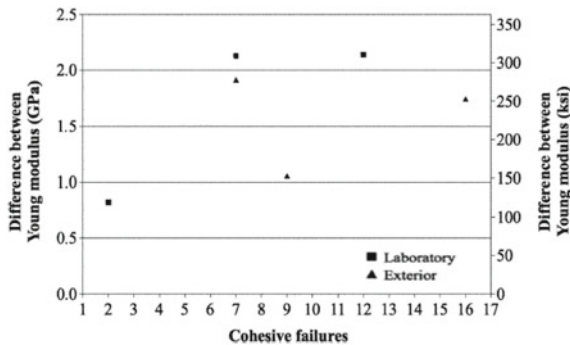
**Fig. 5.26** Failure mode for slant shear test: adhesive (left) and cohesive (right) (Santos and Eduardo Nuno Brito Santos 2011)



these failure modes. Splitting test specimens all presented adhesive failures, while slant shear specimens presented both (Santos and Eduardo Nuno Brito Santos 2011).

The failure mode of a specific element can be influenced by the surface roughness and the compressive strength. First of all, the number of cohesive failures increases when increasing the surface roughness of the interface and this for two curing conditions (lab environment and in-situ environment). Secondly, the failure mode will also be influenced by the compressive strength of the material. The compressive strength of two layers, elaborated on a different time, will be correlated with different Young’s modulus of each layer. Consequently, this varying modulus will induce differential stiffness of the composite concrete member and will change the stress distribution at the interface. Literature showed that the number of cohesive failures increases with the increase of the difference between the Young’s modulus of each concrete layer, as shown in Fig. 5.27. The existence of a correlation between the cohesive failure and the differential stiffness is extremely important because it means that it is possible to change the failure mode of a composite concrete member by designing the differential stiffness between both concrete layers.

**Fig. 5.27** Differential stiffness versus cohesive failures (Santos and Eduardo Nuno Brito Santos 2011)



## 5.5 Durability and Transport Mechanisms in 3D Printed Materials

### 5.5.1 Fire Resistance

Besides the above mentioned mechanical properties of the cementitious material, also the fire resistance plays an important role when implementing 3DP materials in real buildings. Within the Civil and Environmental Engineering Department of IMT Lille, some preliminary fire resistance tests have already been performed on concrete slabs, fabricated with a combination of crushed limestone sand, ordinary Portland cement CEM I 52.5 and superplasticizer to cement ratio equal to 1.5%.

During these tests, two slabs have been extracted from a square test specimen and were placed on top of each other in a concrete frame, covering one side of the gas oven used to apply the thermal stress and soliciting them on one side with a conventional ISO 834–1 time–temperature curve. No mechanical restriction was applied to the edges of the slabs, which could expand freely. The slabs were exposed to fire for more than 120 min and temperature measurements on the unexposed face of the slabs as well as on the plate thermometers in the oven have been performed. The position of the concrete slabs was aligned with the external face of the support wall and thermocouples were fixed on the edges of the slabs (Fig. 5.28) (D’Hondt et al. 2019).

Preliminary test results showed a fire resistance of the material without marked scaling or cracking. The temperature measurements in the oven and on the unexposed side reveal a high thermal gradient (higher than 100 °C/cm) over the thickness of the slab (about 5 cm). This thermal gradient induces a thermal curvature of the slabs with a maximum distortion close to 3 mm (directed towards the oven). Nevertheless, as can be seen on Fig. 5.29, the two slabs seem to be working together while they

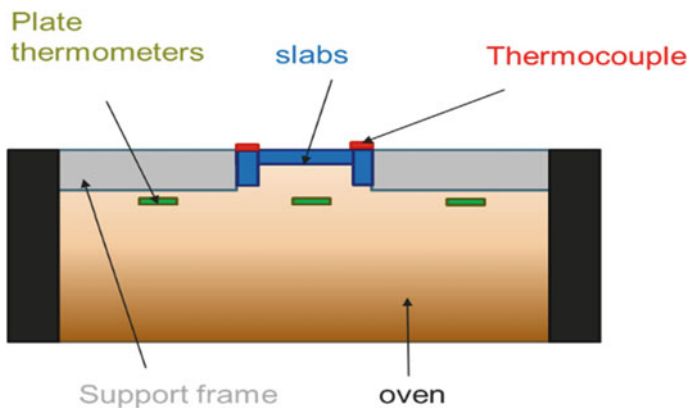
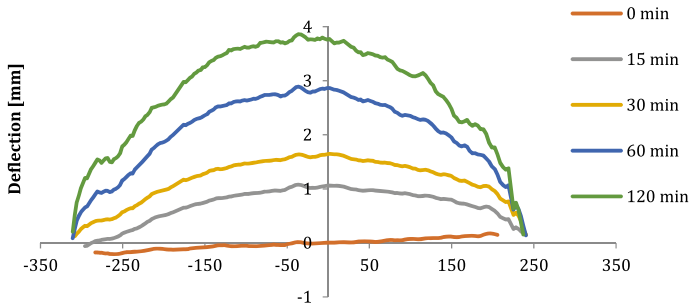


Fig. 5.28 Slab alignment in the oven (D’Hondt et al. 2019)





**Fig. 5.29** Measured concrete slab deflection after different times of fire exposure (D'Hondt et al. 2019)

should be mechanically independent of each other. The material also exhibits a structural integrity and airtightness after 120 min of heating and cooling. The post-cooling observations reveal micro cracks over the height of the slabs, next to the horizontal interfaces. Progressive crumbling characterized by the loss of powdered material on the exposed face has been noticed over time after cooling and storage. All these phenomena occurred on both slabs, suggesting an uniformity of the properties governing the fire behaviour.

Recent research performed at Centre Scientifique et Technique du Bâtiment (CSTB) showed the influence on the compressive strength of printed specimens after fire exposure. The compression tests on these samples were performed perpendicularly and alongside the axis of the cord. According to the test results, the cold material performed a quasi-isotropic behaviour. After fire exposure, a reduction of 73% was obtained when testing the samples alongside the axis of the cord. Due to the high damage level after fire exposure, a compression test perpendicularly to the axis of the cord could not be performed (D'Hondt et al. 2019).

### 5.5.2 Transport Mechanisms

Schröfl et al. (2019) studied water uptake into two formulations of 3D-printed concrete via capillary suction using neutron radiography. The samples varied in their layer-to-layer deposition time intervals and the use of different binders. Time intervals of 2 and 13 min were short enough to avoid preferential capillary suction at interlayer bonding areas in the fine-grained printable concretes containing supplementary cementitious materials. An increase in time interval to 24 h gave rise to quick capillary suction through the layer-to-layer interfaces (Fig. 5.30). However, moisture did not redistribute into the matrix regions from the interfaces. For mixtures with ordinary Portland cement as sole binder combined with an additional superabsorbent polymer (SAP), the short layer-to-layer deposition interval of two minutes resulted in tight interlayer bonds with quasi-null capillary suction. Intervals of 13 and 36 min,

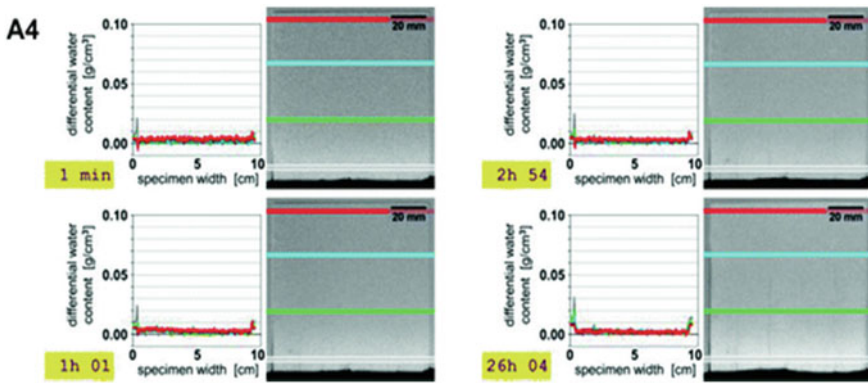


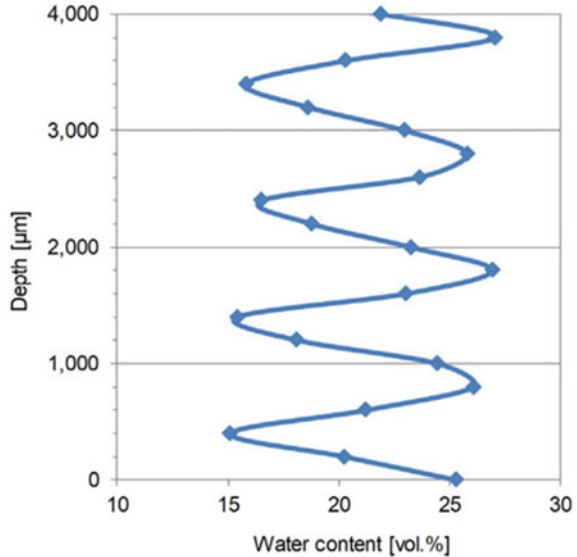
**Fig. 5.30** Differential water content of specimens with one 24 h and three two minute layer-to-layer deposition interval (A19) at four heights indicated in the images and neutron radiography referenced differential images (Schröfl et al. 2019)

however, resulted in partially quick and intense absorption of water and immediate absorption by adjacent SAP particles.

Van Der Putten et al. investigated the effect of different print parameters on the capillary water uptake of multi-layered printed specimens by means of neutron radiography. Within these investigations, two till four layered specimens, fabricated with different printing speeds and/or different mix compositions (with and without the addition of superabsorbent polymers) were exposed to a water basis with different surfaces (bottom and front surface). Preliminary results showed that, when the bottom surface of the samples was exposed to water, no uniform water ingress front could be observed in case of higher printing speeds due to the non-uniform distribution of the sand particles within the bulk material, as proven in other research (Van Der Putten et al. 2019). When the front layer was exposed to the water, all series showed a uniform water ingress front with no preferential water ingress at the interfaces due to a zero minute time gap. The water uptake in the upper layer was always higher due to the lower compaction of this layer during the printing process. For every printing speed and every water exposure surface, compositions with SAPs showed a higher water uptake ability due to the increased porosity of the samples.

Lowke et al. (2015, 2018) showed that using the particle-bed based 3D printing method selective binder (cement) activation, the strength of the material is depending on the water distribution between the layers driven by the surface tension of the water, the adsorption behaviour (Lowke et al. 2018) onto the particle surfaces as well as by capillary force (Boyce et al. 2016). If the amount of water is insufficient, it does not homogeneously penetrate the height of the particle layer. Hence, unhydrated areas remain in deeper parts of the particle layer resulting in a weak layer bonding. In particular at low water-to-cement ratios, insufficient hydrated areas were clearly visible in the cross-section of the printed specimens. To validate this hypothesis, the water distribution over four 1.0 mm layers of an additively printed specimen was determined by one-sided  $^1\text{H}$  NMR (Fig. 5.31). The water content significantly

**Fig. 5.31** Water distribution in the layers determined by one-sided  $^1\text{H}$  NMR spectroscopy (Lowke et al. 2015)



oscillates in accordance with high water content at the top region of the layer and a significantly lower water content at the bottom region (Fig. 5.29). To enhance inter-layer bonding and thus strength, the interlayer water gradient should be minimized by modification of either the particle packing or the water application technique. One method is to increase the water pressure in by jetting the water into particle-bed instead of spraying it onto the surface of the particle-bed.

### 5.5.3 Pore Structure and Porosity

One of the main disadvantages of concrete printing is the fact that voids can form easily between the filaments. This might not only affect the hardened properties significantly, but also the durability of the material as these voids are ideal ingress paths for chemical substances. Only a few researches (Le et al. 2012a; Hambach and Volkmer 2017; Peled and Shah 2003; Shakor et al. 2017) investigated already the creation of voids and the porosity of the printed elements.

Le et al. (2012a) concluded that the pore size distribution is significantly affected by the way elements are produced. The void measurements, showed in Fig. 5.32, were performed by image analyses. The surfaces of different concrete elements (mould cast, poor and good printed specimens) were polished and sprayed with black paint. Once dry, a white paint was rolled on to reveal the voids that retained the black colour. Afterwards, the surface was scanned and the image was transferred to a void measuring software which counted the number of voids in a specific area. As can be seen in Fig. 5.32, the area of small voids (ranging from 0.2–1.6 mm) in

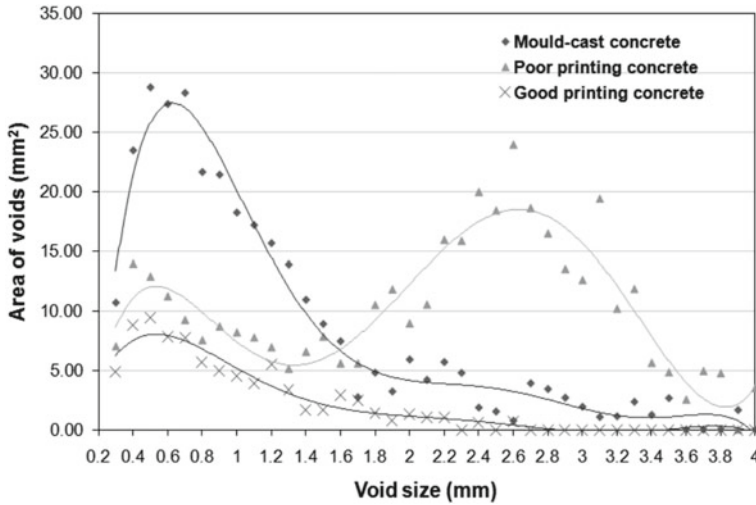


**Fig. 5.32** Distribution of voids in three concrete groups (Le et al. 2012a)

mould-cast concrete is much higher compared to 3D printed elements. The amount of larger voids in poorly printed concrete was significantly higher compared with mould casted concrete and is mostly located between the printed filaments. This is also indicated in Fig. 5.20 (Section ‘Sampling and quality control’). Once these voids can be eliminated, for example by correctly controlling the printing path and concrete rheology, a denser structure can be formed with a smaller amount of voids. The distribution of voids in good printed concrete agreed well with this as the area of 0.2–4 mm voids was significantly lower than both mould-cast and poor printed concrete.

Van Der Putten et al. (2019) investigated intensively the pore structure of printed specimens, manufactured with different time gaps, by means of Mercury Intrusion Porosity measurements (MIP) measurements. For these investigations, drilled specimens were sawn in different pieces to measure the pore distribution of the upper, lower and interlayer separately. First results showed that in case of no time gap, the pore size distribution is comparable for every region. Higher interlayer time intervals not only increased the smaller pores in the centre and lower part of the specimen but also the amount of pores in the upper part. In this research, BSE-SEM analyses were also used for the determination of the pores formed during the hydration process. First observations confirm the above mentioned conclusions. More specifically, in case of a higher time gap, the capillary pores increase due to the moisture exchange between two printed layers with a different moisture content of the layers.

Other researchers (Peled and Shah 2003) investigated not only the effect of the construction process but also the addition of fly ash and fibres by measuring the pore size distribution while conducting Mercury Intrusion Porosimetry (MIP) tests. During these tests, a specific pressure corresponds to an aperture of a pore, and the amount of mercury intrusion approximates to the pores volume. Based on this, the

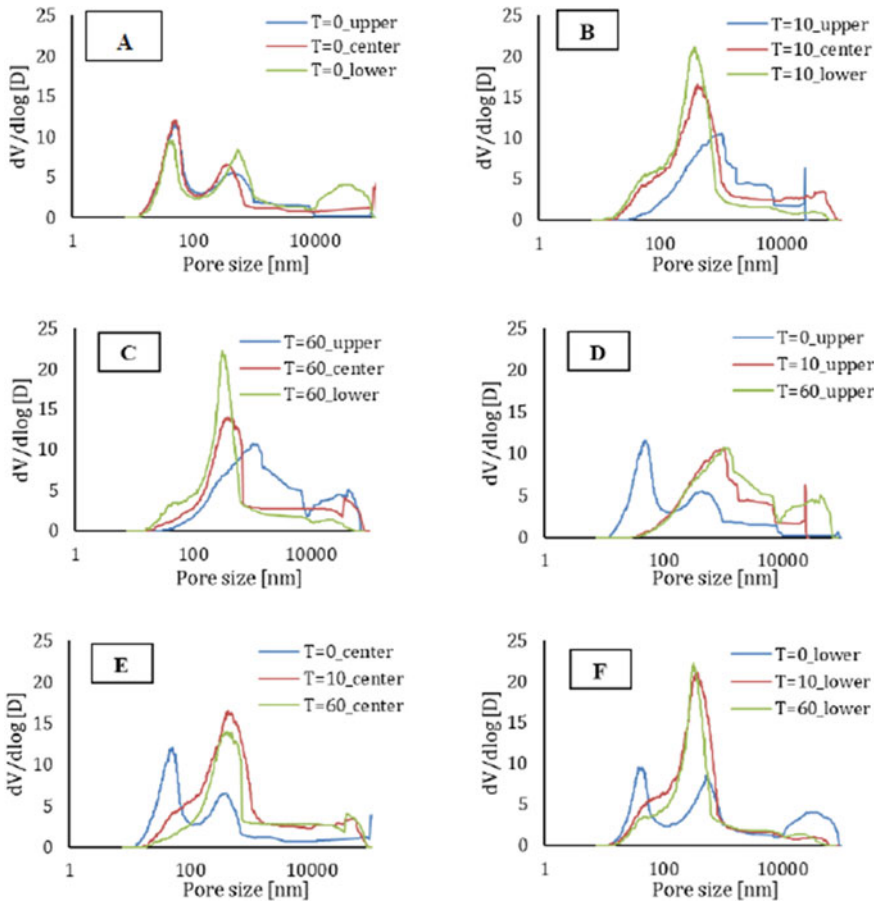


**Fig. 5.33** Pore distribution in different regions of printed specimens, manufactured with increasing time gaps (Van Der Putten et al. 2019)

amount and size of the pores can be determined. Peled and Shah (2003) revealed that the addition of fly ash increases the porosity in all pore ranges (Fig. 5.34a and b). Composites without fly ash are denser and have a lower porosity. This is the case for every fibre type (PVA or acrylic ones).

A similar trend was observed for the cast specimens with and without fly ash. On the other hand, Fig. 5.35 compares the pore size distribution of PVA fibre composites in case of cast and extruded specimens. The extrusion process results in a denser and more compacted composite. The before mentioned differences in porosity between the different construction systems can lead to a stronger matrix and may affect the strength of the fibre-matrix bond. However, it should be kept in mind that MIP measurements determine the pore size distribution of the whole testes specimens, while the porosity and properties at the fibre-matrix interface can differ.

**Fig. 5.34** Pore distribution of extruded and composites with and without fly ash: **a** PVA fibres, **b** Acrylic fibres (Mohammed Sonebibond water-to-binder 2001)

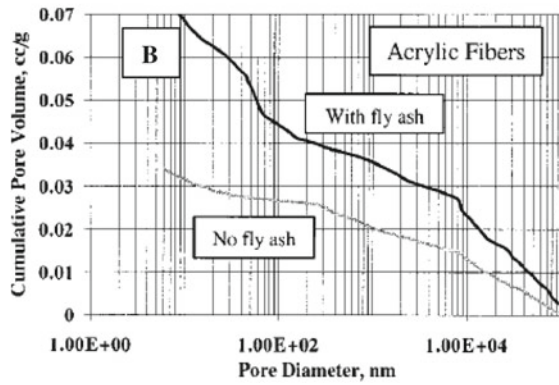
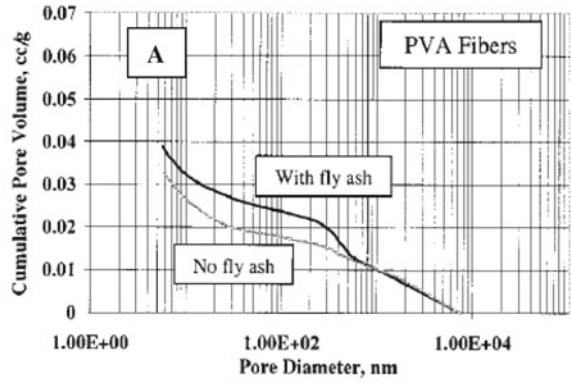
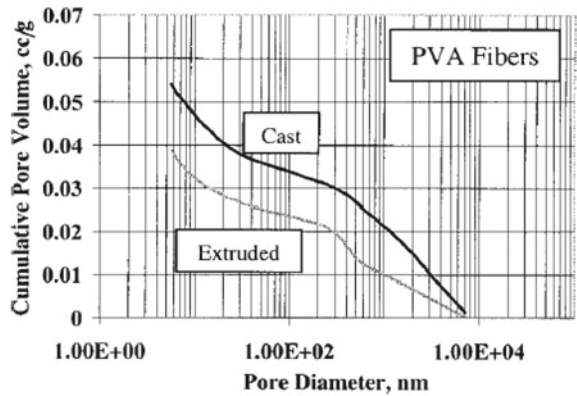


**Fig. 5.35** Pore distribution of extruded and casted composites with PVA fibres (with fly ash) (Mohammed Sonebibond water-to-binder 2001)



Shakor et al. (2017) on the other hand, determined the porosity of the samples using Eq. (5.3). The concrete samples were cast using a specific mix of ordinary Portland cement and calcium aluminate cement. Lithium carbonate was added to some samples in order to reduce the setting time. The porosity measurements were combined with Scanning Electron Microscopy (SEM) analyses to profile the surfaces of the specimens.

$$P_a = \frac{m_3 - m_1}{m_3 - m_2} \bullet 100 \tag{5.3}$$

With:

$P_a$	Porosity	[%]
$m_1$	Weight of the samples after drying for 2 h at 105 °C	[g]
$m_2$	Weight of the samples in soaked water	[g]
$m_3$	Weight of the samples after rolling 4 sides on a damp cloth	[g]

The porosity of the specimens with and without lithium carbonate showed a decreasing trend when increasing the saturation level of the specimens. SEM analyses showed the occurrence of a plate-like large crystal growth which has some other unreacted particles on the surface of the element. Moreover, as shown in Fig. 5.36, there are deep holes and incohesive particles on the SEM figures, which indicate an incomplete hydration between the cement particles. This will consequently have an effect on the mechanical properties of the structure (Fig. 5.37).

Shakor et al. (2017) shows the effect of curing and different saturation degrees on the compressive strength of printed elements composed of a cement mix where ordinary Portland cement was combined with calcium aluminate cement. Increasing the saturation level increases the compressive strength gradually. By increasing the saturation level, total porosity decreases for 3D printed specimens. Maier et al. (2011)

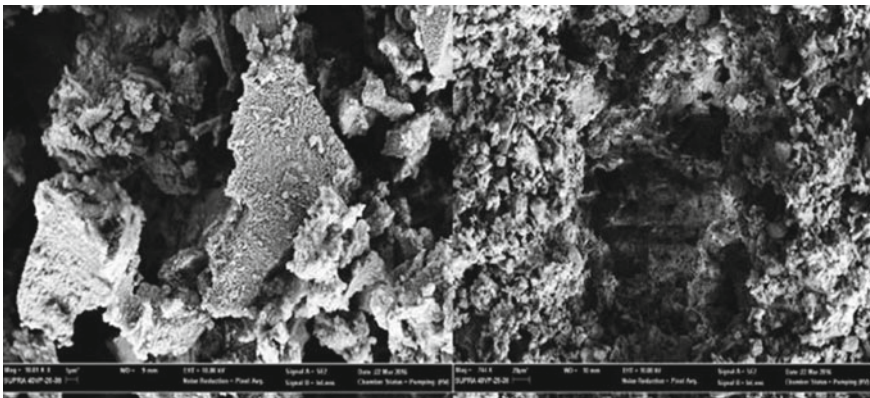
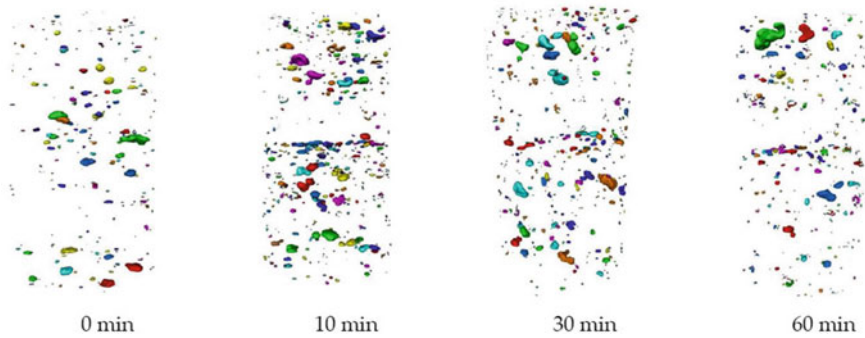


Fig. 5.36 SEM image of 3D printed samples: left (1 μm), right (20 μm) (Shakor et al. 2017)



**Fig. 5.37** 3D rendering of the air voids in 3D printed elements with different time gaps (Van Der Putten et al. 2019)

stated that capillary pores and other large holes are mainly responsible for the reduction in elasticity and strength. They also found that after curing for 72 h, an intermixed crystal network developed and this filled up the pore spaces and minimized the total porosity.

#### 5.5.4 Air Voids

Based on the observations of Van Der Putten et al. (2019), one can conclude that the decreasing strength can be attributed to the lower moisture content of the substrate layer and the higher amount of voids that were induced, resulting in lower adhesion between the printed layers. In case of higher time gaps,  $\mu$ CT-scanning revealed the gathering of air voids at the interface in case, decreasing the overall strength of the printed specimen. These results were also confirmed by Tay et al. (2018), where microscopically investigations of the interlayer showed larger cavities in case of higher time gaps (Fig. 5.38).

Nerella et al. (2017) investigated the effect by Scanning Electron Microscopy (SEM analyses) and classified the interface between the layers into four categories: weakly bonded (a), weakly bonded due to shrinkage or carbonation (b), temporary weakly bonded (c) and strongly bonded (d). Case (a) is when the observed interface between the layers is weakly bonded and is unlikely to be self-healed or bridged by hydration products between the age of 28 days. Case (b) occurs when the observed interface' weak bond can be traced back to plastic, drying shrinkage and/or carbonation rather than to the material rheological properties or time gap. Case (c) represents temporarily weakly bonded interfaces, which are narrow and clearly indicate a self-healing tendency over time due to the build-up of hydration products and in Case (d), the interface between the layers look very similar to reference regions in the core. As expected, the performed time gap between the layers and the applied curing conditions showed a significant influence on the interface quality. Time gaps of 1 day



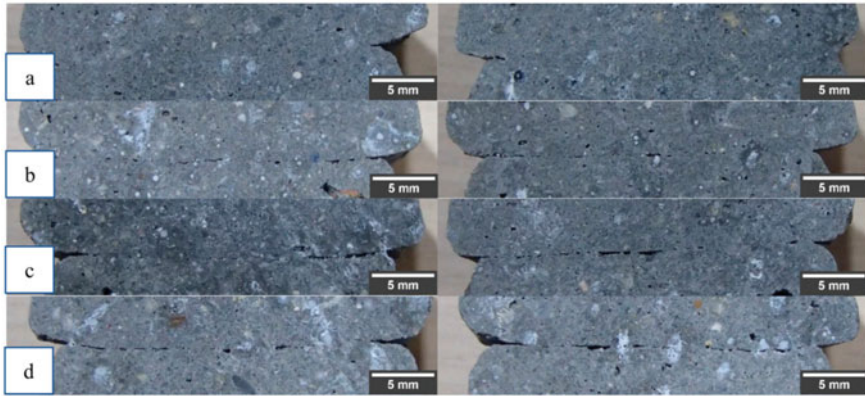


**Fig. 5.38** Samples printed at different time gaps (1, 5, 10 and 20 min) as reported by Tay et al. (2018)

showed the occurrence of cavities and the formation of calcite layers, preventing the development of a proper bonding.

The amount of air voids, entrapped in the cementitious material, not only depend on the interlayer time interval, also the print technique plays an important role as concluded by Nolte (2018) based on CT-scanning. He stated that elements, fabricated by means of a shotcrete principle (i.e. vertical filaments instead of horizontal ones) showed a decreased amount of voids (Fig. 5.40).

### 5.5.5 Carbonation and Corrosion

Dedicated studies on this subject are not yet reported, however, carbonation of printed layers within one day after printing was reported (Nerella et al. 2019) which could have prevented strong interlayer bonding. The concrete composition, surrounding conditions and measured curing influence the carbonation in a significant way. When printed specimens were protected by covering with wet cloths and polythene sheets from the surrounding atmosphere, 3D printed specimens consisting out of a combination of Portland cement, fly ash and micro silica, underwent remarkable carbonation when the applied time interval equals one day. Especially when the top surface of the previous layer (produced one day earlier) showed clear formation of calcites, which prevented it from developing a complete bond with the subsequent layer (Fig. 5.41).

High carbonated specimens were also observed during investigations performed at the university of Ghent and a high dependency on the printing speed and time interval was observed. Within this research, 12 days old four-layered specimens were stored for one week under an increased CO<sub>2</sub> volume of 1%. Visual inspections based on phenolphthalein spray showed that in case of a zero time gap, an uniform carbonation front could be observed for both printing speed. An increased interlayer

time interval increased the carbonation depth in the interlayer between the printed specimens. The dependency of the printed specimens on the applied time gap and printing speed are similar to the capillary water uptake capacity of these specimens as mentioned in Sect. 5.2.

Weger et al. (2018a, b) investigated the carbonation resistance of specimens produced with the particle-bed based 3D printing method selective paste intrusion. For the testing, prisms were printed in Orientation I and II/III and reference specimens were mould-casted. The specimens were stored for one day at 20 °C in the particle bed and the mould, respectively. Afterwards, the specimens were stored at 20 °C under water for seven days. Then, the specimens were stored in standardized conditions (20 °C, 65% R.H.) until the day of testing. One series of specimens was tested in accordance with DIN CEN/TS 12,390–10:2007 under atmospheric conditions after 182 days, another series after 28 days under an increased CO<sub>2</sub> volume of 2%. For the visual identification of the carbonation, phenolphthalein was applied to a freshly broken surface of the specimens. Neither the printed nor the cast specimens showed any carbonation which can be explained by the low water to cement ratio of 0.3.

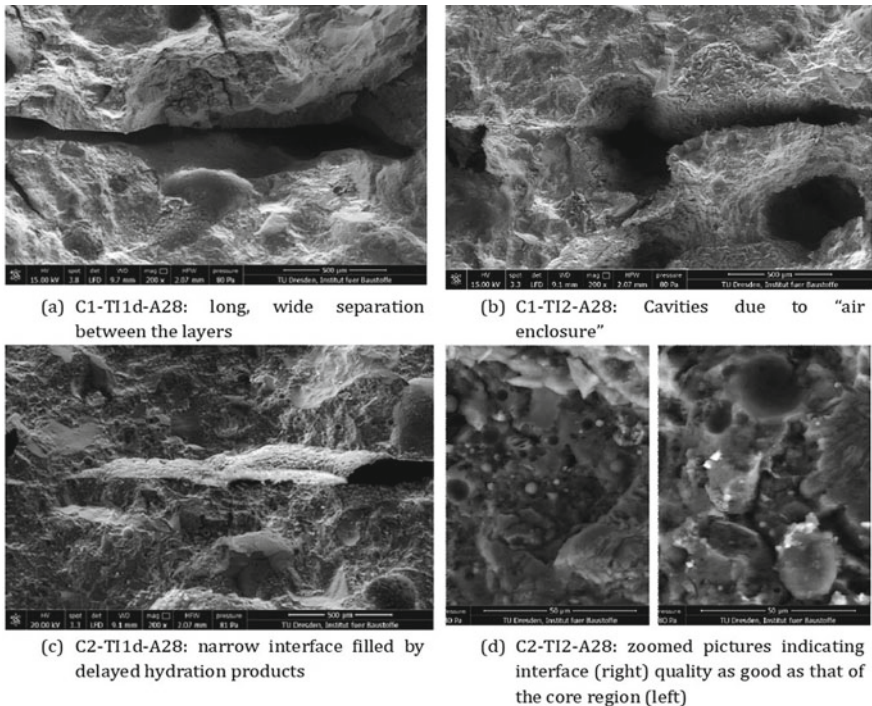
For testing the chloride migration coefficient  $D_{RCM}$ , specimens were produced with the particle-bed based 3D printing method selective paste intrusion. Weger et al. (2018a, b) printed specimens in orientation I and II/III and casted cubes in moulds. The specimens were stored for one day in the particle bed and the mould, respectively. Afterwards, the specimens were stored at 20 °C under water until the 28th day. Within one week before starting of the test procedure, cylinders with a diameter of 100 mm and a height of 50 mm were drilled and sawn from the specimens. At a concrete age of 28 days, the circumference surface of the cylinders was sealed before starting the chloride impact according to (BAW 2017, 2012a, b). The printed as well as the mould-casted reference cylinders showed similar results after 28 days and a resistance to exposure class XF2 and XD2 according to EN 206:2013 + A1:2016 after an age of 56 d and even after 28 days (age of 56 days was only tested with casted specimens). The specimens exhibited no anisotropic behaviour. The results of the casted specimens even almost achieved the limit for exposure class XF3 and XD3 according to EN 206:2013 + A1:2016. The limits for the classification can be found in (BAW 2017, 2012a, b).

### 5.5.6 Freeze–Thaw Resistance

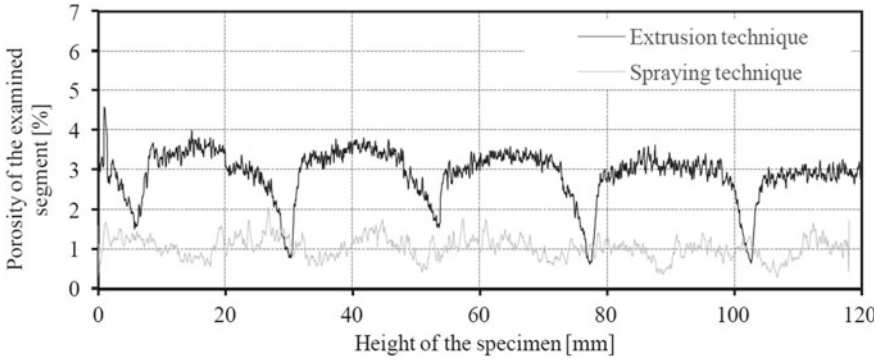
Tian and Han (2018) investigated the effect of different freeze–thaw cycles on the non-air entrained concrete by digital image process (DIP) analysis and mechanical tests. First of all, the porosity of the specimens increased with the increase of freeze–thaw cycles. This implied that the specimens were formed with initial defects, such as pores and micro cracks, and the repeated freeze–thaw actions caused an expansion in volume and movement of the non-frozen water due to hydraulic pressure. These forces induced pore propagation and connection and decreased the durability of the

printed specimen. The pores distribution characteristics showed an increase in bigger pores. The larger pores in the material ruptured were cut through by cracks, forming smaller pores. The higher amount of pores also negatively affected the compressive strength (Fig. 5.38) and created printed specimens with different failure mechanisms (Fig. 5.39). In the first type, the main crack went through the specimen along the diagonal, while in the second type two sets of diagonal cracks appeared on the specimens' centre of height, and cracks propagated quickly (Figs. 5.40, 5.41, 5.42 and 5.43).

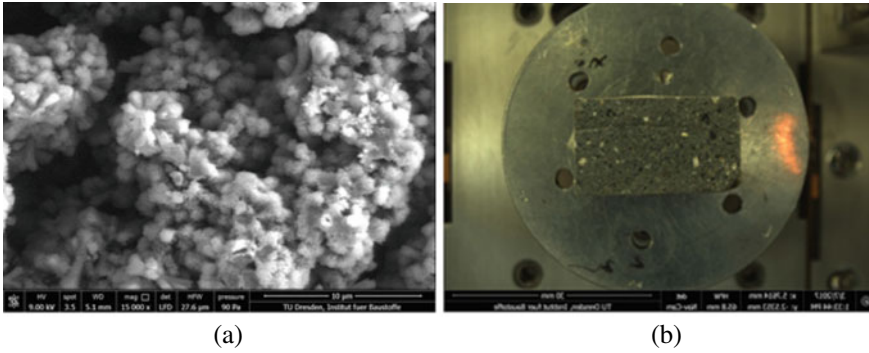
Weger et al. (2018a, b) tested the freeze–thaw-resistance without (CIF) and with (CDF) de-icing salts of specimens produced with the particle-bed based 3D printing method selective paste intrusion. Therefore, specimens were printed in orientation I and II/III and additionally casted as reference test specimens. The specimens were stored respectively one day in the particle-bed and in the mould and afterwards at 20 °C under water until day 7. Thereafter, the specimens were stored until 28 days at a temperature of 20 °C and a relative humidity of 65%. Then, the freeze–thaw resistance was tested according to DIN CEN/TS 12,390–9:2017–05 and was analysed according to (BAW 2018). The printed specimens were tested perpendicular (Orientation I,



**Fig. 5.39** SEM images captured at 28 days concrete age showing the four observed types of layer-interface microstructure of mixtures C1 and C2. TI indicates the time interval (Venkatesh et al. 2017)

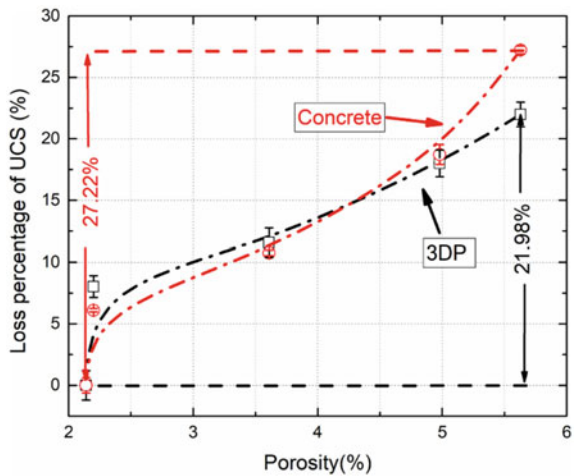


**Fig. 5.40** Pore size distribution of specimens created by spraying or extrusion technique (Nolte et al. 2018)



**Fig. 5.41** **a** Calcite formation at the layer interface and **b** general view of the corresponding specimen (Nerella et al. 2019)

**Fig. 5.42** Relationship between porosity >0.1 mm and loss percentage of uniaxial compressive strengths as reported by Tian and Han (2018)



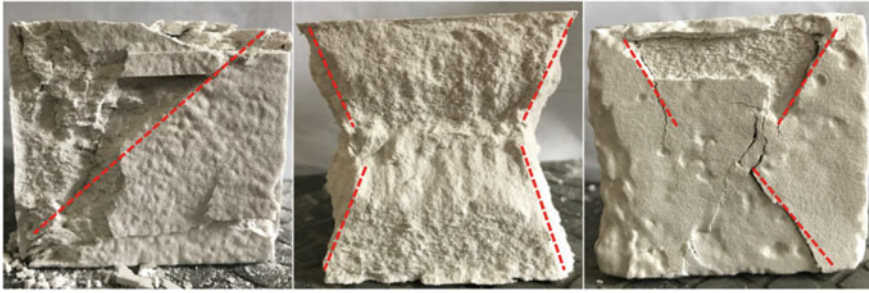


**Fig. 5.43** Failure pattern of 3DP specimens under uniaxial compression

Fig. 5.2) and parallel (Orientation II/III, Fig. 5.2) to the printed layers. The attacked side was not treated and hence the original printed surface. All tested specimens showed high resistance against freeze–thaw attacks without (CIF) and with (CDF) de-icing salts passing even the hardest failure criteria for XF3 and XF4. Additionally, based on the fact that there is no clear tendency in scaling or inner damage depending on the orientation, an isotropic freeze–thaw resistance could be expected.

## 5.6 Recommendations

In order to provide useful support for knowledge development in the engineering community involved in concrete 3D printing activities, technical committees have been recently established among the different international associations, authorities and institutions operating the field of concrete technology or, in general, of construction materials. The research outcomes concerning properties and testing of printed materials/structures in the fresh/hardened state are commonly discussed in these international working group and technical documentation for supporting testing and design are expected to be released in the coming years.

Among these and in addition to the 276-DFC committee (Digital fabrication with cement-based materials) established by RILEM in 2016, the FIB (Fédération Internationale du Béton) has recently opened the activities of Task Group 2.11: Structures made by Digital Fabrication which mainly focus on the mechanical behaviour of manufactured structures rather than on the aspects related to the technological processes; following this, the primary objective consists in identifying and overcoming the limitations of the current design practice for the implementation of novel, digitally-fabricated concrete structures. Preliminary activities deal with the following topics: mechanical behaviour of printed elements in the hardened state; reinforcement strategies; structural design approaches for digitally fabricated elements. The American Concrete Institute (ACI), a leading authority involved in concrete design, construction, and materials, has also launched the committee ACI

564: 3D Printing with Cementitious Materials with the objective of developing technical documentation on the ways additive manufacturing may be integrated into the concrete community. This technical group is currently working on the collection of available/applicable reinforcing and anchoring systems for Additively Constructed Concrete (ACC), including passive reinforcement (e.g. reinforcing bars, fibre reinforcement, interface reinforcement, print ties/stabilizers); active reinforcement (e.g. internal prestressing, external prestressing); alternative reinforcing (e.g. cables, FRP etc.).

## References

- al., B.e. (2019). The effect of Superabsorbent polymers on the Mitigation of Plastic Shrinkage Cracking of Conventional Concrete, Results of a RILEM inter-laboratory test by TC 260-RC. Under submission, Materials and Structures.
- Asprone, D., et al. (2018). Rethinking reinforcement for digital fabrication with concrete. *Cement and Concrete Research*, 112, 111-121.
- Aysha, H., et al. (2014). An overview of interface behaviour between concrete to concrete. *International Journal of Advanced Structures and Geotechnical Engineering*, 03(02), 110-114.
- (BAW), B.f.W. (2017). BAW Merkblatt Dauerhaftigkeitsbemessung und -bewertung von Stahlbetonbau-werken bei Carbonatisierung und Chlorideinwirkung (MDCC).
- (BAW), B.f.W. (2012a). BAW Code of Practice - Resistance of Concrete to Chloride Penetration (MCL).
- (BAW), B.f.W. (2012b). BAW Merkblatt Dauerhaftigkeitsbemessung und -bewertung von Stahlbetonbau-werken bei Carbonatisierung und Chlorideinwirkung (MDCC).
- (BAW), B.f.W. (2018). BAW Merkblatt: Frostprüfung von Beton (MFB): Ausgabe 2012.
- Bos, F., et al. (2016). Additive manufacturing of concrete in construction: potentials and challenges of 3D concrete printing. *Virtual and Physical Prototyping*, 11(3), 209–225.
- Boyce, C., Ozel, A., and Sundaresan, S. (2016). Intrusion of a Liquid Droplet into a Powder under Gravity. *Langmuir*, 32.
- Beushausen, H., and Alexander, M. G. (2007). Localised strain and stress in bonded concrete overlays subjected to differential shrinkage. *Materials and Structures*, 40(2), 189-199.
- Beushausen, H., and Alexander, M. G. (2008). Bond strength development between concretes of different ages. *Magazine of Concrete Research*, 60(1), 65–74.
- Bos, F. P., et al. (2017). Experimental Exploration of Metal Cable as Reinforcement in 3D Printed Concrete. *Materials (Basel, Switzerland)*, 10(11), 1314.
- Christ, S., et al. (2015). Fiber reinforcement during 3D printing. *Materials Letters*, 139, 165-168.
- Curosu, I., et al. (2017). Tensile behavior of high-strength strain-hardening cement-based composites (HS-SHCC) made with high-performance polyethylene, aramid and PBO fibers. *Cement and Concrete Research*, 98, 71-81.
- D'Hondt, M., et al. (2019). Fire behavior of a printed sample for building. in *Dixite 3D Print*. 2019. Champs-sur-Narme.
- Di Carlo, T. (2012). Experimental and numerical techniques to characterize structural properties of fresh concrete relevant to contour crafting. University of Southern California California, p. 196.
- Emmons, P. H., and Emmons, B.H. (1993). Concrete Repair and Maintenance Illustrated: Problem Analysis; Repair Strategy; Techniques, in *Concrete Repair and Maintenance Illustrated: Problem Analysis; Repair Strategy; Techniques*, p. 314.
- Feng, P., et al. (2015). Mechanical properties of structures 3D printed with cementitious powders. *Construction and Building Materials*, 93, 486-497.

- Hambach, M., and Volkmer, D. (2017). Properties of 3D-printed fiber reinforced Portland cement paste. *Cement and Concrete Composites*, 79, 62-70.
- Hack, N., et al. (2017). MESH MOULD: AN ON SITE, ROBOTICALLY FABRICATED, FUNCTIONAL FORMWORK.
- Hack, N., and Lauer, w. v. (2014). Mesh-Mould: Robotically Fabricated Spatial Meshes as Reinforced Concrete Formwork. *Architectural Design*, 84.
- Júlio, E. N. B. S., Branco, F. A. B., and Silva, V. T. D. (2004). Concrete-to-concrete bond strength. Influence of the roughness of the substrate surface. *Construction and Building Materials*, 18(9), 675-681.
- Kumarji, S., and Geneidy, O. (2019). <http://www.iaacblog.com/tag/concrete-3d-printing/>.
- Le, T. T., et al. (2012a). Hardened properties of high-performance printing concrete. *Cement and Concrete Research*, 42(3), 558-566.
- Le, T. T., et al. (2012b). Mix design and fresh properties for high-performance printing concrete. *Materials and Structures*, 45(8), 1221-1232.
- Lloret, E., et al. (2017). SMART DYNAMIC CASTING SLIPFORMING WITH FLEXIBLE FORMWORK -INLINE MEASUREMENT AND CONTROL
- Liu, Z., et al. (2019). Interlayer Bond Strength of 3D Printing Cement Paste by Cross-Bonded Method. *Journal of the Chinese Ceramic Society*, 47(5), 648-652.
- Lowke, D., et al. (2015). 3D-Drucken von Betonbauteilen durch selektives Binden mit calciumsilikatbasierten Zementen – Erste Ergebnisse zu betontechnologischen und verfahrenstechnischen Einflüssen.
- Lowke, D., et al. (2018). Particle-bed 3D printing in concrete construction – Possibilities and challenges. *Cement and Concrete Research*, 112, 50-65.
- Marchment, T., et al. (2017). Effect of delay time on the mechanical properties of extrusion-based 3D printed concrete, in 34th Interenational Symposium on Automation and Robotics in Construction. Taiwan.
- Mechtcherine, V., et al. (2019). Large-scale digital concrete construction – CONPrint3D concept for on-site, monolithic 3D-printing. *Automation in Construction*, 107, 102933.
- Maier, A. -K., et al. (2011). Three-dimensional printing of flash-setting calcium aluminate cement. *Journal of Materials Science*, 46(9), 2947-2954.
- Mechtcherine, V., et al. (2014). Effect of internal curing by using superabsorbent polymers (SAP) on autogenous shrinkage and other properties of a high-performance fine-grained concrete: results of a RILEM round-robin test. *Materials and Structures*, 47(3), 541-562.
- Mohammed Sonebibond water-to-binder. (2001). r., Effect of Silica Fume, Fly Ash and Water-to-Binder Ratio on Bond Strength of Underwater, Self-Consolidating Concrete. *ACI Symposium Publication*, 199.
- Mechtcherine, V., et al. (2018). 3D-printed steel reinforcement for digital concrete construction – Manufacture, mechanical properties and bond behaviour. *Construction and Building Materials*, 179, 125-137.
- Nerella, V. N., Hempel, S., and Mechtcherine, V. (2019). Effects of layer-interface properties on mechanical performance of concrete elements produced by extrusion-based 3D-printing. *Construction and Building Materials*, 205, 586-601.
- Nerella, V. N., et al. (2016). Studying printability of fresh concrete for formwork free Concrete on-site 3D Printing technology technology (CONPrint3D), in *Rheol. Messungen an Baustoffen 2016 - Tagungsband Zum 25. Workshop und Kolloquium*, pp. 236-246.
- Neville, A. M. (1995). *Properties of concrete*. Vol. 4. 1995: Longman London.
- Nematollahi, B., et al. (2018). Effect of Type of Fiber on Inter-Layer Bond and Flexural Strengths of Extrusion-Based 3D Printed Geopolymer. *Materials Science Forum*, 939, 155-162.
- Nolte, N., et al. (2018). Schichtenverbund bei der additiven Fertigung-Einflussgrößen und Verfahrensvergleich.
- Ogura, H., Nerella, V. N., and Mechtcherine, V. (2018). Developing and Testing of Strain-Hardening Cement-Based Composites (SHCC) in the Context of 3D-Printing. *Materials (Basel)*, 11(8).

- Paul, S. C., et al. (2018). Fresh and hardened properties of 3D printable cementitious materials for building and construction. *Archives of Civil and Mechanical Engineering*, 18(1), 311–319.
- Panda, B., Chandara Paul, S., and Jen Tan, M. (2017). Anisotropic mechanical performance of 3D printed fiber reinforced sustainable construction material. *Materials Letters*, 209, 146–149.
- Panda, B., et al. (2018). Measurement of tensile bond strength of 3D printed geopolymers mortar. *Measurement*, 113, 108–116.
- Perrot, A., Rängeard, D., and Pierre, A. (2016). Structural built-up of cement-based materials used for 3D-printing extrusion techniques. *Materials and Structures*, 49(4), 1213–1220.
- Pierre, A., et al. (2018). Penetration of cement pastes into sand packings during 3D printing: analytical and experimental study. *Materials and Structures*, 51(1), 22.
- Peled, A., and Shah, S. P. (2003). Processing Effects in Cementitious Composites: Extrusion and Casting. *Journal of Materials in Civil Engineering*, 15(2), 192–199.
- Rahul, A. V., et al. (2019). Mechanical characterization of 3D printable concrete. *Construction and Building Materials*, 227, 116710.
- Rubio, M., et al. (2019). Mechanical properties of 3D bio-printing cement-based materials. in *Third International Conference on “Bio-Based Building Materials (ICBBM)*. Belfast.
- Roussel, N., and Cussigh, F. (2008). Distinct-layer casting of SCC: The mechanical consequences of thixotropy. *Cement and Concrete Research*, 38, 624–632.
- Sanjayan, J. G., et al. (2018). Effect of surface moisture on inter-layer strength of 3D printed concrete. *Construction and Building Materials*, 172, 468–475.
- Santos, D. S., Santos, P. M. D., and Dias-da-Costa, D. (2012). Effect of surface preparation and bonding agent on the concrete-to-concrete interface strength. *Construction and Building Materials*, 37, 102–110.
- Santos, P. M. D., and Eduardo Nuno Brito Santos, J. (2011). Factors Affecting Bond between New and Old Concrete. *Materials Journal*, 108(4).
- Serpukhov, I., and Mechtcherine, V. (2015). Early-Age Shrinkage of Ordinary Concrete and a Strain-Hardening Cement-Based Composite (SHCC) in the Conditions of Hot Weather Casting, pp. 1504–1513.
- Schröfl, C., Nerella, V. N., and Mechtcherine, V. (2019). *Capillary Water Intake by 3D-Printed Concrete Visualised and Quantified by Neutron Radiography*. 2019. Cham: Springer International Publishing.
- Shakor, P., et al. (2017). Modified 3D printed powder to cement-based material and mechanical properties of cement scaffold used in 3D printing. *Construction and Building Materials*, 138, 398–409.
- Tay, Y. W. D., et al. (2018). Time gap effect on bond strength of 3D-printed concrete. *Virtual and Physical Prototyping*, 14, 104–113.
- Tian, W., and Han, N. (2018). Pore characteristics (>0.1 mm) of non-air entrained concrete destroyed by freeze-thaw cycles based on CT scanning and 3D printing. *Cold Regions Science and Technology*, 151, 314–322.
- Van Zijl, G.P.A.G., S.C. Paul, and M.J. Tan. (2016). Properties of 3D Printable Concrete, in *2nd International Conference on Progress in Additive Manufacturing*, Singapore.
- Van Der Putten, J., et al. (2019a). Microstructural Characterization of 3D Printed Cementitious Materials. *Materials*, 12(18).
- Van Der Putten, J., et al. (2019b). 3D Printing of cementitious materials with superabsorbent polymers, in *Durable Concrete for Infrastructure under Severe Conditions - Smart Admixtures, Self-responsiveness and Nano-additions*. Ghent, pp. 86–89.
- Van Der Putten, J., De Schutter, G., and Van Tittelboom, K. (2019). Surface modification as a technique to improve inter-layer bonding strength in 3D printed cementitious materials. *RILEM Technical Letters*, 4(0).
- Venkatesh, N., Hempel, S., and Mechtcherine, V. (2017). Micro- and macroscopic investigations on the interface between layers of 3D printed cementitious elements, in *International Conference on Advances in Construction Materials and Systems*. Chennai.



- Wang, Z. W. L., and Zhao, X. (2018). Apparatus and method for preparing a building structure with 3d printing, C.C.N.I.P.A.R.f. <https://patents.google.com/patent/US20200391409A1/en?inventor=zhendi+wang&oq=zhendi+wang>, Editor.
- Wangler, T., et al. (2016). Digital Concrete: Opportunities and Challenges RILEM Technical Letters, 1, 67–75.
- Weger, D., Lowke, D., and Gehlen, C. (2016a). 3D printing of concrete structures using the selective binding method – Effect of concrete technology on contour precision and compressive strength, in 11th fib International PhD Symposium in Civil Engineering, A.K.a.J.Y. K. Maekawa, Editor. Tokyo, pp. 403–410.
- Weger, D., Lowke, D., and Gehlen, C. (2016b). 3D Printing of Concrete Structures with Calcium Silicate based Cements using the Selective Binding Method - Effects of Concrete Technology on Penetration Depth of Cement Paste, in 4th International Symposium on Ultra-High Performance Concrete and High Performance Construction Materials 2016, Kassel University Press: Kassel
- Weger, D., Gehlen, C., and Lowke, D. (2018a). Additive Fertigung von Betonbauteilen durch selektive Zementleim-Intrusion.
- Weger, D., et al. (2018b). Additive manufacturing of concrete elements using selective cement paste intrusion-effect of layer orientation on strength and durability in RILEM 1st International Conference on Concrete and Digital Fabrication. Zürich.
- Wolfs, R. J. M., Bos, F. P., and Salet, T. A. M. (2019). Hardened properties of 3D printed concrete: The influence of process parameters on interlayer adhesion. Cement and Concrete Research, 119, 132–140.
- Wyrzykowski, M., et al. (2018). Recommendation of RILEM TC 260-RSC: using superabsorbent polymers (SAP) to mitigate autogenous shrinkage. Materials and Structures, 51(5), 135.
- Zareiyan, B., and Khoshnevis, B. (2017). Interlayer adhesion and strength of structures in Contour Crafting - Effects of aggregate size, extrusion rate, and layer thickness. Automation in Construction, 81, 112–121.
- Zareiyan, B., and Khoshnevis, B. (2017). Effects of interlocking on interlayer adhesion and strength of structures in 3D printing of concrete. Automation in Construction, 83, 212–221.
- Zingg, A., et al. (2009). Interaction of polycarboxylate-based superplasticizers with cements containing different C3A amounts. Cement and Concrete Composites, 31(3), 153–162.